Streamlining river groynes

Laboratory experiments in schematised geometry under submerged flow conditions

Bram Langeveld

TU Delft

Rijkswaterstaat

Streamlining river groynes

Laboratory experiments in schematised geometry under submerged flow conditions.

MSc thesis. Final version.

Author:
Bram Langeveld

Thesis committee:

Prof. dr. ir. W.S.J. Uijttewaal	Delft University of Technology
Dr. ir. E. Mosselman	Delft University of Technology & Deltares
Dr. ir. B. Hofland	Delft University of Technology
Dr. ir. A. Sieben	Rijkswaterstaat

Date: June 22, 2023

Cover: Aerial photograph of groynes in the river Waal and the Pannerdensch canal. (Rijkswaterstaat)

TU Delft Rijkswaterstaat

Acknowledgements

I would like to express my gratitude to my thesis committee. First and foremost, to Wim Uijttewaal for personally guiding me through the process of my master thesis, for giving me the freedom to develop myself, for the weekly meetings with very helpful feedback and discussions and for the good communication throughout the months. Furthermore, I would like to thank Arjan Sieben, Erik Mosselman and Bas Hofland for giving helpful feedback during the progress meetings and visiting me while I was working on my experiment. I also want to thank the lab technicians Pieter, Chantal, Arie, Arno and Frank for helping me with the measurement equipment and modifying the model set-up during my experiment.

Summary

Groynes are hydraulic structures commonly applied in the Dutch rivers. Depending on the water depth, groynes can be emerged or submerged. When a groyne is emerged, it has two main functions: maintaining the water depth in the main channel and preventing the river from eroding its bank. When the discharge in the river increases, the groynes become submerged. A submerged groyne acts as an obstacle to the flow, resulting in additional resistance and an increase in the upstream water level.

To increase the flow capacity of a river during extreme conditions, a couple of measures can be considered: increasing the height of the dikes and embankments, reducing the overall resistance of the river cross-section and increasing the area of a river cross-section.

This thesis focuses on reducing the overall resistance of the river cross-section, and more specifically, on investigating the effect that streamlining the downstream slope of a groyne has on the groyne-induced resistance. Hypothetically, streamlining the groyne by decreasing its downstream slope would decrease the intensity of flow processes like downstream flow separation, which could increase the discharge capacity of the groyne, and thus of the river cross-section, as a result of the decrease in groyne-induced resistance. An increase in discharge capacity would decrease the flood risk during extreme conditions.

To investigate the effect of streamlining a groyne by decreasing its downstream slope, a physical model experiment was set up in the $5 \times 40\ m^2$ flume at the Hydraulic Engineering Laboratory of Delft University of Technology. The physical model represents part of a river cross-section. From the total $5\ m$ width, the main channel and groyne field both took up $2\ m$ and the floodplain took up $1\ m$. In streamwise direction, the flume contained six groynes and five full groyne fields. The groyne fields had transverse bed slope of 1:25. Electromagnetic flow meters (EMF meters) were used to measure the flow velocity at many points in both streamwise and transverse direction. The water level was measured by laser altimeters.

Decreasing the downstream slope of a groyne to 1:8 compared to a reference situation with a downstream slope of 1:3 resulted in a 4 % increase of the discharge capacity over the crest of the groyne. This increase of discharge capacity was not uniform over the transverse axis. Near the groyne tip, this increase of discharge capacity was more than 6 %, whereas at the end of the groyne, the discharge capacity decreased slightly compared to the reference situation.

A more detailed analysis of the data gave insight in why decreasing the downstream slope of a groyne increases the discharge capacity of a groyne. Streamlining the groynes resulted in a significant decrease of the relative turbulence intensity along the downstream slope of the groyne. This was consistently around 50 % lower for the streamlined groynes compared to the reference situation, indicating less intense turbulent structures. Moreover, auto-correlation functions of the flow velocity signals showed a shorter correlation length in conjunction with lower amplitudes and smaller periods of the fluctuations for the streamlined groynes. This indicates a signal with less correlation and higher frequencies. These results explain why the discharge capacity of a streamlined groyne is larger than of a reference groyne.

Contents

List of symbols

This list of symbols gives an overview of the symbols that are used multiple times in the text of this report. Symbols that only occur in figures and/or equations are explained locally and do not show here. The page number on the right shows where the symbol is used for the first time.

Symbol	Unit	Meaning	Page
C	$[m^{1/2}/s]$	Chézy coefficient	42
C_d	$[-]$	Discharge coefficient	4
C_{d0}	$[-]$	Discharge coefficient in case of free flow over the crest	7
D_{n50}	$[m]$	Median nominal stone size	43
Fr	$[-]$	Froude number	17
h	$[m]$	Water depth relative to the crest height	5
H	$[m]$	Energy head relative to the crest height	4
H_0	$[m]$	Reference height	7
H_t	$[m]$	Total water depth	9
k_s	$[m]$	Bed roughness height	42
L_k	$[m]$	Crest width	4
n	$[s/m^{1/3}]$	Manning coefficient	13
q	$[m^2/s]$	Specific discharge	7
Q	$[m^3/s]$	Discharge	17
R	$[m]$	Hydraulic radius	43
Re	$[-]$	Reynolds number	17
s	$[-]$	Submergence level of a weir/groyne	6
z_u	$[m]$	Crest height of a groyne	7

1 | Introduction

Groynes are hydraulic structures commonly applied in the Dutch rivers. A groyne is a short, rubble mound structure in the river bed, constructed at an angle to the flow direction to deflect the flow away from critical zones, like the river banks. In order to normalise the flow, they are usually constructed every couple of hundred metres on both sides of the river. Figure 1.1 shows an image of groynes in the river Waal and the Pannerdensch canal.

Figure 1.1: Aerial photograph of groynes in the river Waal and the Pannerdensch canal, (source: Rijkswaterstaat).

During normal flow conditions, the groynes are emerged. The main function of groynes is twofold. First, groynes make for a uniform width of the main channel. This decreases the gradients in the flow velocity which results in a more uniform water depth in the main channel. The fact that a more uniform cross-section of the main channel usually coincides with a decrease in conveyance width, also increases the flow velocity, which leads to less sediment accumulation in the main channel. This means that less maintenance in needed to keep the river bed at its required depth. The larger flow velocity also reduces the amount of ice build-up in the river during cold periods. The second function of groynes is to prevent natural meandering as a result from bank erosion.

During extreme discharge events, the groynes will submerge and become part of the conveyance area of the river. Now, the groynes act as obstacles that add additional resistance to the flow. In the case of the Dutch rivers, over the past century, the crest height of the groynes remained constant while the river bed level decreased. This causes an additional increase in groyne-induced resistance compared to the original situation.

Two methods to decrease groyne-induced resistance is to either lower or streamline the groynes. The resulting decreased resistance will in turn lead to a lower water level and a lower risk of flooding during an extreme discharge event. Streamlining of groynes might be preferable over lowering of groynes due to the fact that the height of the groynes relative to the river bed is directly related to the effect the groyne has on maintaining the required depth of the main channel, i.e. lowering of groynes might lead to additional sediment accumulation in the main channel, and become submerged more often. A streamlined groyne

has a milder downstream slope than a reference groyne. The hypothesis behind this is that a milder downstream slope will decrease the amount of flow separation downstream of the groyne, which will in turn decrease the overall resistance inflicted by the groyne.

Decreasing the crest height of a groyne is a method that has already been applied along certain areas along the Dutch river system as part of the Room for the River program. At this moment, streamlining groynes has not yet been applied and is considered as an option for the Pannerdensch canal.

The current methodology to quantify the effect of groyne streamlining is to use D-Hydro. This is a numerical model for two-dimensional horizontal flow solving the 2D shallow water equations. In D-Hydro, energy loss over a groyne is modelled as a head loss over a weir in a subgrid process. This is a simplification of reality, as flow over and around a groyne is more complicated than flow over a weir. For flow over a weir the head loss is mainly determined by the flow contraction upstream and the flow expansion downstream of the weir. The head loss from a groyne is also influenced by various other processes, like flow around the groyne tip and momentum exchange in the horizontal mixing layer between the main channel and the groyne field.

To get more insight in flow around groynes, Delft University of Technology and Rijkswaterstaat have set up a physical model experiment in the $5 \times 40\ m^2$ flume in the Hydraulic Engineering Laboratory of the faculty of Civil Engineering and Geo-sciences of the Delft University of Technology. In this flume, part of a cross-section of a river is constructed with a geometric scaling of 1:30. This cross-section represents a section of the river Waal and contains part of the main channel, six groynes, five groyne fields and a part of the floodplains.

1.1 Problem description

In principle it is well known that decreasing the resistance of groynes will have a positive effect on reducing flood risk by increasing the overall discharge capacity of the river (e.g. Yossef, 2004).

The problem that arises when investigating streamlining groynes using numerical models, is the fact that the hydraulic effect of streamlining is unknown. This can result in unreliable results from numerical models. Due to this lack of data, groynes are often schematized as weirs or applied as an additional resistance parameter in a subgrid model (Ambagts, 2019). For example, D-Hydro adds additional resistance as a result of flow separation when the bed slope is steeper than 1:7 (Sieben, 2003). This makes it difficult to accurately quantify the effect the adjustments have on the flow resistance.

1.2 Research objective and goals

The objective of this research is to gather experimental data on the effect that streamlining of groynes has on the reduction of the overall resistance of the river. In this thesis, the gathered data is used to get better insight in the flow processes over and around groynes and the horizontal mass and momentum exchange in the mixing layer between the main channel and the groyne field in this physical model set-up and to explain how these model results will represent real-world scenarios. Regarding the problem description and the research objectives stated above, the following research goals are formulated:

- Quantify the change in overall water level slope in the river section and display the results in such a way that it is possible to draw clear and objective conclusions regarding the effectiveness of streamlining groynes in rivers.
- Use the gathered flow velocity data from the scaled river section, and more specifically from around the groyne tip, to get better insight in, and to analyse the flow over and around groynes and to draw conclusions on how this flow differs for streamlined groynes compared to reference groynes.

1.3 Reading guide

After this introduction, chapter 2 gives an overview of the relevant literature regarding flow over and around submerged groynes. This includes information about methods to approximate flow over and around groynes using better understood and better researched flow processes like flow over a weir. Furthermore, to compliment the problem statement from section 1.1, some uncertainties observed in literature regarding using numerical models to investigate the effect of streamlining groynes are given.

Chapter 3 is a detailed description of the methodology used in this research. This includes some basic information on the set-up of the model, the hydraulic conditions for which the measurements are conducted, a description of the measurement techniques and an overview of all the measurement locations.

Following the research methodology, chapters 4 and 5 present the results following from the measurements. The results are divided into two chapters to distinct between the two measurement techniques (water levels and flow velocities).

The discussion in chapter 6 starts with an uncertainty analysis. This is important to give the reader a sense of the accuracy and applicability of the gathered data set. Furthermore, in chapter 6 two methods are compared to get an estimation of the bed roughness in the main channel part of the flume. Last, the limitations of the model set-up are presented and the results are compared to the available literature (which were also mentioned in chapter 2.

In chapter 7, the conclusions and recommendations are presented.

2 | Literature study

This chapter gives an overview of the relevant theory behind the flow over and around groynes. This research focuses on submerged groynes. This is due to the fact that the effect of streamlining groynes will only be visible and relevant during extreme conditions, i.e, submerged groynes. Therefore, emerged groynes will not be considered for this literature study.

2.1 Flow over and around a submerged groyne

As stated in chapter 1, groynes become submerged during high-discharge events. This means they become part of the conveyance area of a river cross-section. Subsequently, this adds resistance to the flow compared to a situation without groynes. This section gives an overview of the various flow processes that are associated with flow over and around a groyne.

These flow processes are: weir-like flow regimes over the crest of the groyne; vertical flow separation downstream of the groyne crest resulting in rotating flow over the vertical, i.e. wake formation; momentum exchange in the horizontal mixing layers between the main channel and the groyne fields and between the groyne fields and the floodplain; flow around the groyne tip; eddy formation behind the groyne tip and flow characteristics in a series of groynes.

2.1.1 Flow regimes over a weir

A weir is defined as a simple hydraulic structure, e.g, a low, submerged dam, that is usually constructed perpendicular to the flow direction in a river or canal, with the purpose of increasing the upstream water level or to regulate the flow.

The most well known schematization of the flow over a weir is given by Hoffmans (1992). Hoffmans defined three regions for the flow over a weir. These are the acceleration zone, the transition zone and the deceleration zone. Figure 2.1 illustrates this concept.

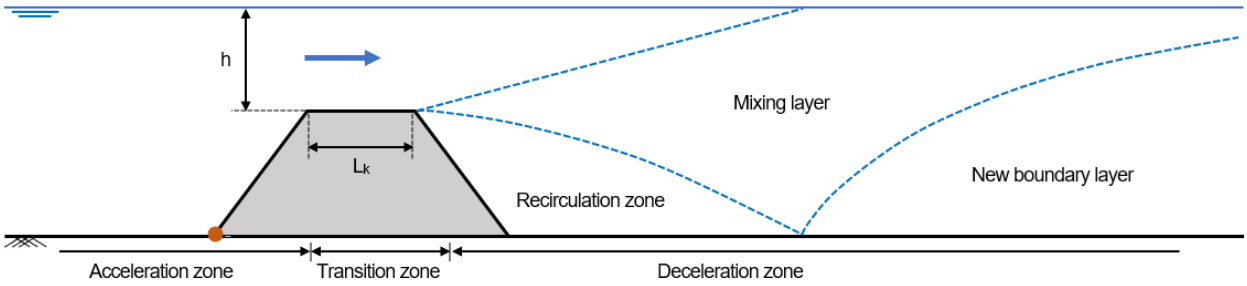

Figure 2.1: The different stages of flow over a weir according to Hoffmans (1992). Note that the water level in this figure does not represent the actual water level for flow over a weir. In a real-world scenario, the water level would look similar to the water level in figure 2.4.

Acceleration zone

At the upstream side of the weir, the flow accelerates. This means that the velocity head will increase and the water level related to the original bed level will decrease. The manner in which this happens depends on upstream slope of the weir and the curvature of the bed at the red dot in figure 2.1.

If this slope and curvature are sufficiently mild, the accelerating and converging flow profile will develop over the entire water depth. If the curvature at the red dot and the upstream slope of the weir become steeper, eventually conditions will be such that the converging flow can not fully develop over the entire water depth. This will lead to a local reduction in flow velocity near the red dot caused by non-hydrostatic effects (Sieben, 2003). According to Malekzadeh *et al.* (2022), who researched the effect of various weir parameters, e.g. crest height, slope angles *etc.*, on the discharge coefficient C_d of the weir, upstream flow separation will start to have significant impact when the weir has an upstream slope steeper than 30°. The groynes used for this research will have an upstream slope of around 1:3, which corresponds to roughy 18°. Therefore, it is assumed that upstream flow separation will not have a significant effect on the results of this research.

Transition zone

The horizontal crest of the weir is a transitional region of flow between the acceleration zone and the deceleration zone. Weirs can be classified based on the Froude number and the length of the crest. When the Froude number over the crest is larger than one, the flow is supercritical and independent of downstream conditions, called a perfect weir. A Froude number below one results in subcritical flow and the flow is dependent on both the upstream and downstream conditions, called an imperfect weir.

The length of the crest determines whether the weir is categorized as long or short. On a long-crested weir, a new logarithmic flow profile will develop on the weir crest. Over a short crested weir, such a logarithmic flow profile has not enough space to develop. This has implications for the discharge capacity of the weir. Long-crested weirs can have a lower discharge capacity than short crested weirs. Research from Bos (1989), Fritz and Hager (1998) and Brater and King (1976) agree that a weir is defined as short crested when the ratio of H/L_k is larger than 1.

For this research the crest width L_k is 3 cm and the water depth relative to the crest height h is equal to 10 cm. This means a short crested groyne during all tests. The Froude number will be sufficiently small as to ensure subcritical flow conditions representative for the Dutch river system.

Deceleration zone

A mixing layer develops at the start of the deceleration zone. This mixing layer separates two areas with different flow velocities. In a situation with relatively small water level slopes, the fast moving layer lies above the slowly moving layer. This highly turbulent, slow moving layer, also called the recirculation zone, results from separation of the flow due to the sharp downstream slope of the weir. If this downstream slope becomes sufficiently mild, the flow stays attached to the slope and the decelerating and diverging flow profile will develop over the entire water depth. This decreases the resistance over the weir.

In this research, a downstream slope of 1:3 represents the current situation where there is flow separation and a downstream slope of 1:8 represents the situation where there is no flow separation downstream.

2.1.2 Horizontal momentum exchange

In accordance with the straight uniform compound channel model, studied by van Prooijen (2004), two regions with different flow velocities in the horizontal plane, e.g. the main channel and groyne fields, exchange momentum via a turbulent mixing layer. The presence of this mixing layer will increase the hydraulic resistance of the river compared to a theoretical situation without a turbulent mixing layer. This

will lead to a reduction in discharge capacity which is also known as the kinematic effect (Barishnikov en Ivanov, 1971). Figure 2.2 shows the velocity distribution between two regions of different flow velocity.

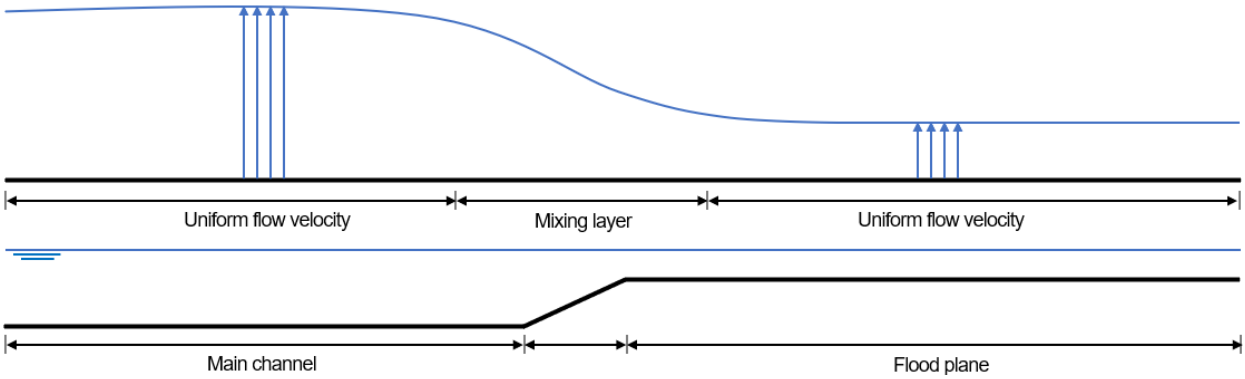

Figure 2.2: Velocity distribution between two regions of different flow velocity.

This transverse exchange of momentum via a turbulent mixing layer is caused by the mean flow and turbulence (van Prooijen, 2004). The mean flow contribution is twofold: first is the effect of the depth-averaged downstream and lateral velocities and second is the advective dispersion, i.e. vertical variation of these velocities (van Prooijen, 2004). The mixing layer is characterised by small scale turbulence caused by bottom friction and large-scale turbulence caused by the lateral shear stress between the two regions of different flow velocity, as shown in figure 2.2.

Among other things, these processes result in large-scale vortical motions. When considering two regions with a different flow velocity and also a different water level, the water level will vary along the diameter of the vortical structures. This causes acceleration and deceleration of this vortical structures as the water depth varies. Figure 2.3 is an illustration of this concept.

It should be noted that these researches focused on effects of a horizontal mixing layer in a straight and uniform compound channel and did not include the effect of groynes. The groynes are expected to complicate the principle behind the mixing layer as a groyne, and especially a series of groynes, causes a disturbance in the bed level, which contradicts the assumption of a uniform channel.

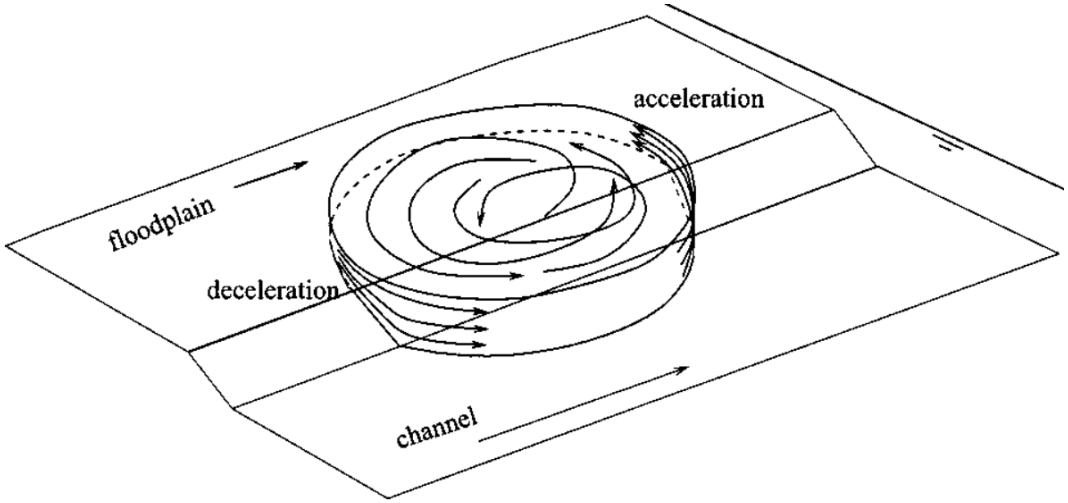

Figure 2.3: Large-scale vortical structures as a result of turbulent mixing layers. Source: van Prooijen (2004).

The concept of horizontal momentum exchange between two flow regions with different velocities has been well researched and documented over the past decades. For more detailed explanations regarding this concept, refer to the research of van Prooijen *et al.* (2005), Sofialidis and Prinos (1999), Alavian and Chu (1985) and Knight and Shiono (1990).

2.1.3 Flow around the groyne tip

Because a groyne does not span the entire width of a river cross-section, water can flow both over the crest and around the groyne tip. Flow around the groyne tip is caused by a transverse water level slope in front of the groyne when looking in the direction of flow. Considering a transact in front of the groyne, the water level in front of the groyne is higher than in the main channel, causing water to flow towards the main channel around the groyne tip.

As stated by Harms (2021), little research is available that focuses specifically on flow around the groyne tip. This complements the problem statement from section 1.1, that due to a lack of understanding and experimental data, it is possible that one of these flow processes is (partially) responsible for the inaccurate estimation of the resistance of groynes in the numerical models.

2.2 Streamlining the downstream slope of a weir-like structure

The aim of this research is to investigate the effect of streamlining the downstream slope of groynes under submerged conditions. Remarkable is the abundance of research regarding flow over unsubmerged weirs and the lack of research for submerged weirs. Sieben (1999) assumed that the effect of a milder downstream slope for a submerged weir with subcritical flow could not be reliably quantified due to a lack of experimental data. Based on this conclusion, Delft University of Technology performed a couple of experiments on a trapezoid-shaped weir-like structure in a flume at the Hydraulic Engineering Laboratory (Bloemberg, 2001). The main question of these experiments was whether the energy loss inflicted by the weir-like structure could be reduced by a milder downstream slope. Figure 2.4 gives an overview of the parameters used to define the weir and the hydraulic conditions in the flume during the experiments from Bloemberg (2001).

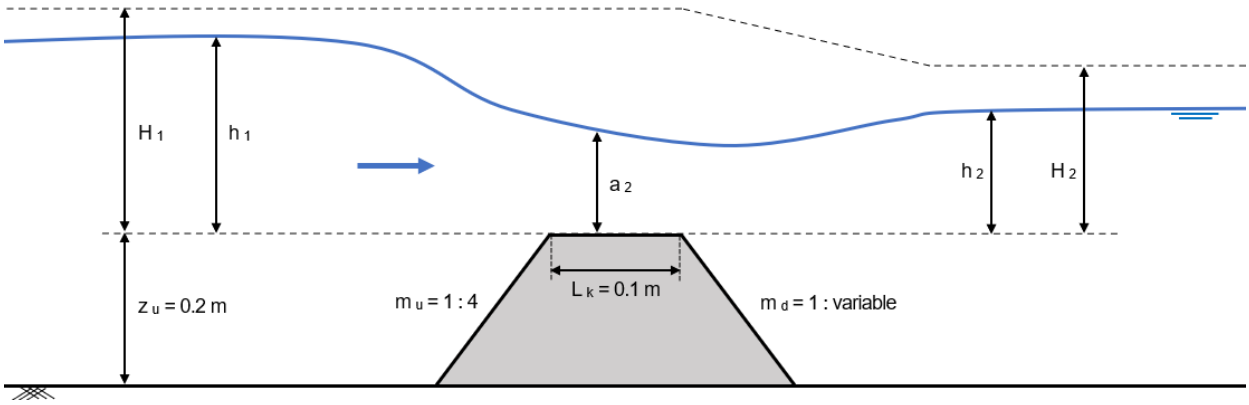

Figure 2.4: Overview of the parameters of the weir and hydraulic conditions.

Bloemberg (2001) plotted the calculated discharge coefficients resulting from the water level measurements against the submergence level $s = h2/h1$. This discharge coefficient was calculated using equation 2.1 for four different downstream slopes.

$$C_d = \frac{3\sqrt{3}}{2\sqrt{2}} \frac{q}{\sqrt{g} H_0^{3/2}} \tag{2.1}$$

The plotted data is displayed in figure 2.5. From this figure it can be concluded that for larger values of s, i.e. lower Froude numbers, the discharge coefficient seemed to increase for a milder downstream slope. This shows the positive effect that streamlining has on the discharge capacity of the weir-like structure.

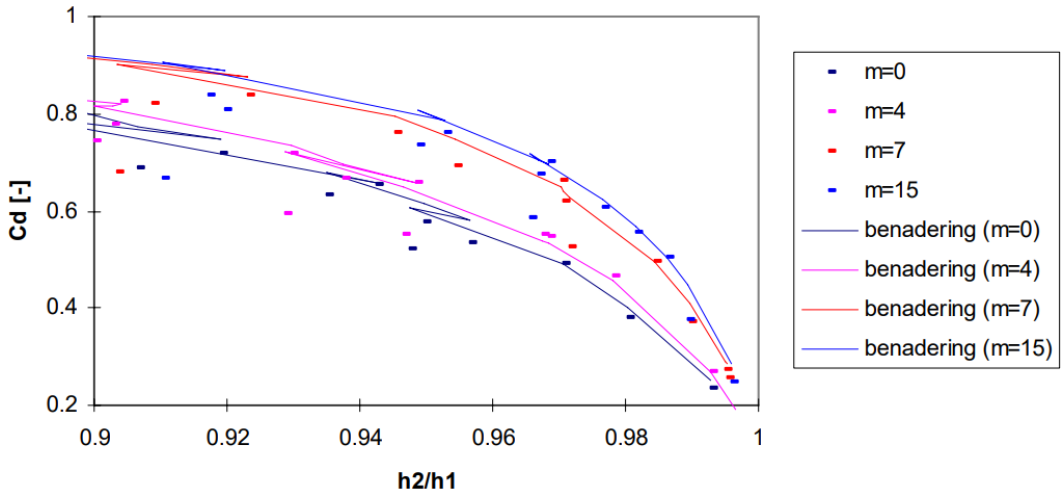

Figure 2.5: Discharge coefficient plotted as a function of the submergence level s. The continuous lines represent a theoretical approximation of the data using an adjusted form of the Villemonte approach. In this figure, m corresponds with the steepness of the downstream slope. Figure source: Sieben (2003). Data source: (Bloemberg (2001).

Combining the measurement results from Bloemberg (2001) with theory and experiments from Bazin (1888) and Brater and King (1976) will lead to the following discharge relation for a weir-like structure.

$$q = C_{d0} \frac{2\sqrt{2}}{3\sqrt{3}} \sqrt{g}\, H_1^{3/2} \sqrt{1 - (H_2/H_1)^p} \tag{2.2}$$

C_{d0} [-] is the discharge coefficient in case of free flow over the crest. This coefficient is estimated by the following formula.

$$C_{d0} = 0.85 \left(\exp^{-0.15 H_1/L_k} \left(1 - 0.25 \exp^{-0.5 m_u}\right) + \left(1 - \exp^{-0.15 H_1/L_k}\right) \left(0.8 + 0.65 \exp^{-0.1 m_d}\right) \right) \tag{2.3}$$

The coefficient p is estimated by $p = 11 + 1.6\, m_d$, which only depends on the downstream slope.

It is important to be aware of the application range of this discharge relation. Equation 2.2 and 2.3 were calibrated using experimental research performed by Bloemberg (2001). Bloemberg (2001) used a model of a weir with geometric scaling of 1:30 and the downstream slope varied from a vertical wall to slopes of 1:4, 1:7 and 1:15. The Froude number at the crest of the weir was varied from 0.1 to 1.0. The upstream Froude number varied from 0.03 to 0.18. The upstream slope, the crest width (L_k) and the crest height (z_u) remained constant, with values of 1:4, 0.1 m and 0.2 m respectively. The downstream water depth (h_2) was varied 0.04 m to 0.15 m.

This discharge relation can be expanded to account for the elevation difference in crest height and downstream bed level. This expansion is relevant for research regarding flow over a weir-like structure with low Froude numbers, i.e. below 0.15, e.g. flow in the Dutch river system. However, for reasons explained in 3.3.2, this expansion is less relevant for this research as the Froude numbers on the groyne crests are higher, i.e. around 0.25 to 0.3. Furthermore, Sieben (2003) stated that while the theoretical fit of this method was good, comparing the theoretical results with actual field data obtained by Rijkswaterstaat in 1968 showed that the scatter was too large to identify a relation.

The effect of streamlining a weir can be illustrated using the discharge relation described in equations 2.2 and 2.3. The experiments in this research are focused around streamlining the downstream slope of a groyne while keeping the other groyne parameters equal. Figure 2.6 shows the results of streamlining the downstream slope of a weir with a small relative crest length ($H_1/L_k = 1.0$, figure 2.4) using equations 2.2 and 2.3, which are calibrated on the experimental research of Bloemberg (2001).

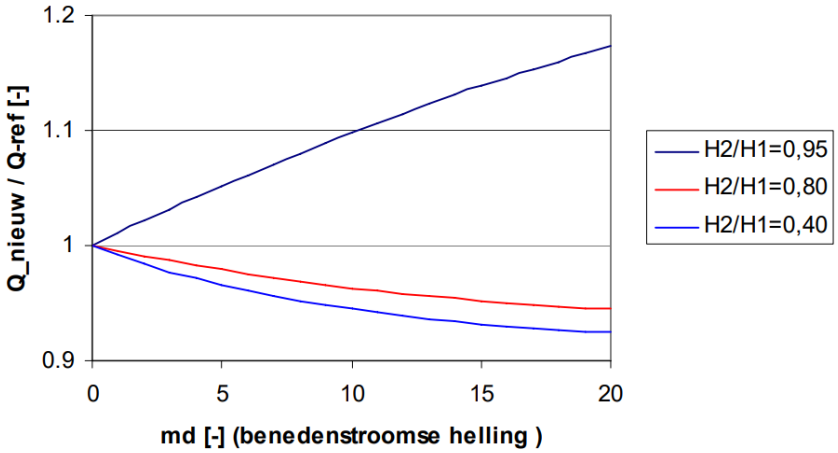

Figure 2.6: Result of streamlining the downstream slope of a weir. The y-axis represents the ratio of the new discharge (which follows from streamlining the downstream slope) to the reference discharge. The x-axis is in correspondence with the downstream slope angle. Source: Sieben (2003).

Figure 2.6 shows that streamlining the downstream slope of a short crested weir in case of a high submergence level ($H_2/H_1 \geq 0.90$) increases the discharge capacity. In the case of a lower submergence level, a decrease in discharge capacity is expected.

In this thesis, the downstream slope of the groynes is varied from 1:3 to 1:8. Based on figure 2.6, the increase in discharge over the crest of a weir-like structure would then be around 4-5 %, given a submergence level of $H_2/H_1 = 0.95$.

2.3 Groyne resistance approximation

Yossef (2004) tried to approximate the resistance of a groyne and find a relation between the resistance and the submergence level. The experiments done by Yossef (2004) were carried out in the same flume that is used for this thesis, with a slightly different bed geometry, e.g. no floodplain and a flat bed in the groyne field.

For the analysis of his data, Yossef (2004) approximated the groynes as roughness elements in the flow. He stated that there are two sources of resistance in the groyne regions: bed resistance and groyne-inflicted resistance. With this information, the momentum balance equation per unit width in the groyne region is

written as equation 2.4. For the full explanation of this approach, refer to Yossef (2004).

$$total\ resistance = bed\ resistance + groyne\ resistance \rightarrow ghi = \frac{g}{C_{base}^2}\, u_{gr}^2 + \frac{1}{2}\, C_d \left(\frac{z_u}{S}\right)\, u_{gr}^2 \tag{2.4}$$

In this equation, h is the local water depth; i is the local water level slope; C_{base} can be approximated by the Chézy value in the main channel; u_{gr} is the depth-averaged flow velocity at a location in the groyne field where the influence of the horizontal mixing layer is not present; z_u is the groyne height and S is the spacing between two groynes.

The absence of the influence of a transverse slope in the groyne field and the absence of a floodplain and accompanying mixing layer causes the applicability of this formula to be limited for the experiments of this thesis, but can give valuable insight nonetheless.

Figure 2.7 below shows there is a correlation between the discharge coefficient normalised with the Froude number squared and the blockage ratio of a groyne (groyne height z_u over total water depth H_t). The normalisation of the discharge coefficient over the Froude number made it possible to eliminate the effect of the different hydraulic conditions.

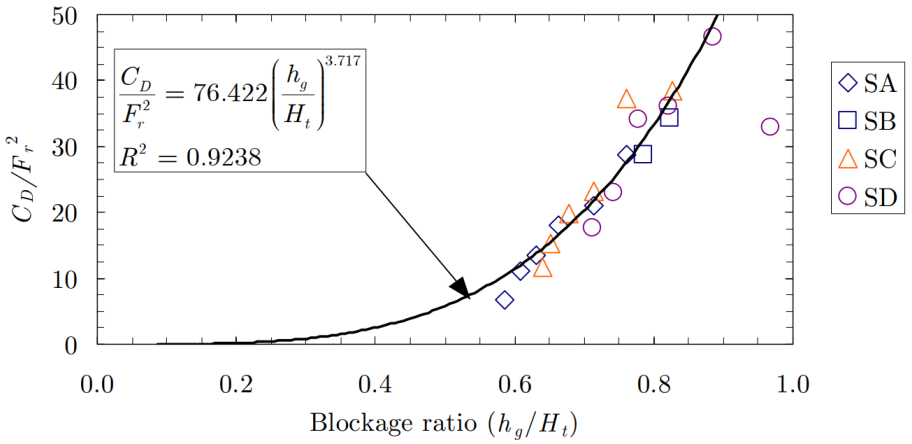

Figure 2.7: Relation between the normalised discharge coefficient and the blockage ratio. The black square with the arrow shows the relation that can be used to calculate the discharge coefficient within the application range of the experiments. 'SA', 'SB', 'SC' and 'SD' denote the different test cases for which various hydraulic conditions were applied. Source: Yossef (2004).

Just as in section 2.2, it is important to be aware of the application range and the limitations of this relation. The experiments were carried out in a $5 \times 40\ m^2$ flume with the model having a geometric scaling of 1:40. The Froude number in the main channel varied from 0.08 to 0.28. The up and downstream slope of the groynes remained equal to 1:3. Throughout the experiments, the total water depth H_t varied from 0.25 m to 0.35 m. Note that the experiment of Yossef (2004) was specifically set up to investigate the effect the submergence level has on the resistance of a groyne.

2.4 Applicability of groyne approximations

Section 2.3 only shows the research of Yossef (2004) on the approximation of the groyne resistance. Kruijt (2013) compared multiple research reports related to this topic. In order to compare each formula, a 1D model of a single groyne in an infinitely long groyne field was considered. He used all the proposed discharge and drag relations proposed by these reports and plotted the discharge coefficient (C_d) as a function of the water depth ratio (H_t/z_u, i.e. water depth over groyne height). The results are displayed in figure 2.8 below.

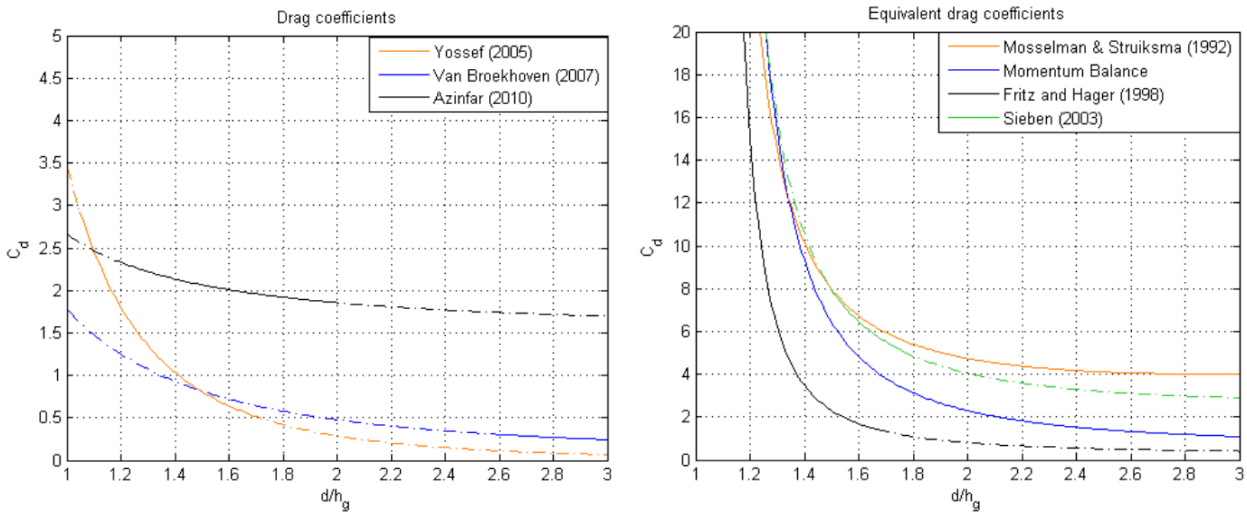

Figure 2.8: Relations of the discharge coefficient over the water depth ratio from all the compared research evaluated by Kruijt (2013). The left graph shows the results of the drag resistance approximations. The right graph shows the results of the weir approximations. The solid part of the lines in both the left and right graph represent the ranges for which these relations were validated. Source: Kruijt (2013).

From figure 2.8 it is concluded that the difference between these formulas is large, up to a factor of five in some cases. The weir approximations consistently overestimate the discharge compared to the drag approximations (Kruijt, 2013). This is because the weir approximations assume all discharge to pass over the crest of the groyne. This means these formulas are very sensitive to water depth over groyne height ratios (H_t/z_u) close to 1 as they will approach infinity.

Based on the formulas plotted in figure 2.8, Kruijt (2013) assessed how these discharge coefficients behaved while varying different parameters they depend on. For a detailed explanation on every parameter that is varied, refer to chapter 3 of the thesis of Kruijt (2013). An important conclusion he drew from comparing these formulas is that none of the considered methods could be used to represent groynes in a 1D schematized model. The most common problems he found were related to the formulas being applied outside their applicable and validated range, unwanted parameter scaling or unexplained oddities within the formulas themselves. For example, the formula of Yossef (2004) shown in figure 2.7 is dependent on the main channel Froude number. However, there is no explanation given for why this should be the case.

This might also support the problem statement from section 1.1, i.e. there is indeed a gap in the knowledge regarding flow over and around groynes or how this flow pattern relates to the proposed approximations discussed in section 2.2.

2.5 Modelling submerged groynes

When analysing various reports regarding the impact of groynes on the flow in a river, it becomes clear that it is possible that various numerical researches draw completely different conclusions while investigating the same problem under slightly different conditions. This section discusses multiple researches regarding this topic and the problems or shortcomings that arose while comparing them. The researches considered are from Van Schijndel & Jagers (2001), Van Broekhoven (2007), Kruijt (2013), Ambagts (2019) and Chavarrías (2022).

The most notable contradictory was between Ambagts (2019) and Kruijt (2013). Ambagts (2019) concluded that his numerical models underestimate the resistance of groynes in a river cross-section. He also concluded that for lower submergence levels, a groyne shows better resemblance to a weir than for higher submergence levels. On the other hand, Kruijt (2013) concluded that a groyne is better represented by a weir for higher submergence levels. In contrast to Ambagts (2019), Chavarrías (2022) concluded that numerical models overestimate the resistance of groynes.

The following subsections elaborate on some key aspects of modelling the effects of groynes.

2.5.1 Availability of experimental data

The first problem is related to the amount of available experimental and field data for these numerical researches. Most of the numerical models set up to investigate the flow over and around submerged groynes are tailored to a specific case. Van Broekhoven (2007) focused his research on the effect that lowering the crest height of groynes has on the discharge capacity of the river, while Van Schijndel & Jagers (2001) and Ambagts (2019) tried to find how their numerical models could represent reality as accurately as possible, if at all. Van Broekhoven (2007) and Kruijt (2013) had no experimental data available for their numerical calibrations, only statistical data regarding the discharge and the water levels in a certain section of a river. Van Schijndel & Jagers (2001) used experimental data from research conducted by Delft University of Technology. In this experiment, flow velocities were measured in one groyne field along four transacts in x-directions, twelve points in y-direction and two points in z-direction. The locations of the transacts in x-direction give a sufficient data coverage to analyse the flow in a groyne field for a situations with emerged groynes, but do not allow a significant data coverage for flow over submerged groynes (as there is no data acquired around the groynes themselves). The fact that only two flow velocities were measured in the z-direction complicated the calculation of the depth-averaged flow velocity, which Van Schijndel & Jagers (2001) used for the flow velocity graphs resulting from their numerical model.

It is not a certainty that the results of these numerical models would be more reliable or that the calibration of these numerical models would be more effective in a situation with more experimental data. However, more experimental data would help the modeler to get a better understanding of the flow characteristics that play a role in the region of interest he or she tries to approach using the numerical models.

The lack of experimental and field data available for numerical models is a problem observed throughout multiple researches. Uijttewaal (2005) stated that flow data from field experiments is rare or problematically accessible.

Recently, Harms (2021) gathered a large data set regarding flow over and around submerged groynes. This data set included flow velocity data in streamwise and transverse direction and water level data. Chavarrías (2022) used this experimental data to compare to the output of his numerical model. He found

large deviations between the numerical model and the experimental data. Chavarrías (2022) was unable to draw decisive conclusions as he stated the accuracy of the measurements was insufficient to allocate these deviations to an actual physically related disagreement between the experiment and the model. Chavarrías' (2021) claim about measurement inaccuracies was complemented by results from the experimental data itself, as a plot of the total discharge in the flume showed an increase of the total discharge over the length of the flume. This is physically impossible given a constant discharge at the upstream boundary of the flume. Figure 2.9 is a visual representation of this problem.

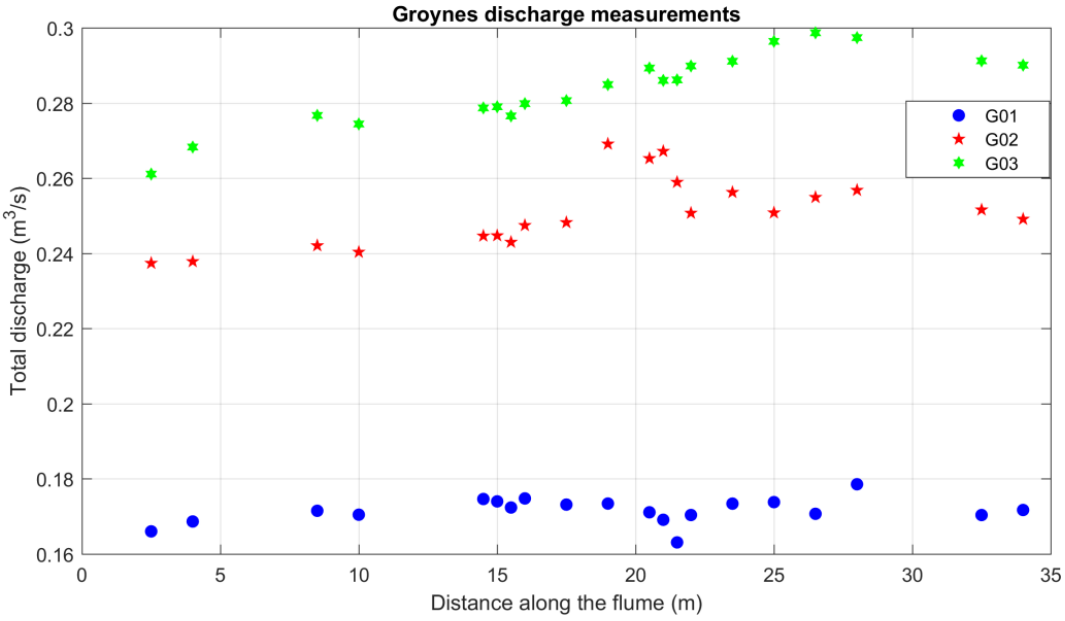

Figure 2.9: Total discharge as a function of longitudinal direction of the flume. Source: Chavarrías (2022).

It should be noted that the flow velocity and water level data from Harms (2021) were point measurements taken in a large flume. This means that a lot of inter- and extrapolation was needed to obtain the discharge in the flume. This can lead to errors unrelated to the measurement accuracy, but more so to the inter- and extrapolation techniques or to the number of measurements being insufficient. However, this will probably not solve the problem of the increasing discharge over the length of the flume, but it is an example to show that it might be unfair to just blame the measurement accuracy.

2.5.2 Bed roughness

The second problem one faces with numerical modelling of submerged groynes is related to various model parameters, e.g. the upstream discharge or velocity boundary, the bed roughness of the model and the grid size of the model.

Van Broekhoven (2007) experienced issues with the calibration of the bed roughness of the model. The only information available to van Broekhoven (2007) was the upstream discharge, the resulting water level slope, the downstream water level and the bed geometry of the area. When imposing the discharge boundary upstream, he found a significant deviation in the resulting water level slope from the model compared to the actual situation. Van Broekhoven (2007) blamed this deviation on the bed roughness in the floodplain that was too low. To solve this issue, van Broekhoven (2007) had to impose a roughness height that was larger than the actual water depth, which is conceptually impossible. Of course, such a large bed roughness is the result of vegetation and buildings within the floodplain. A workaround for the problem

was to reduce the width of the floodplain. Reducing the width of the floodplain might influence the lateral exchange of mass and momentum between the main channel, the groyne fields and the floodplain. However, van Broekhoven (2007) did not investigate this phenomenon.

Harms (2021) conducted a series of measurements to determine the friction in a flume representing a river bed. Without going into detail here, he concluded that a Manning coefficient equal to $0.026\ s/m^{1/3}$ was best to represent the mean conditions. When calibrating these results for his numerical model, Chavarrías (2022) observed large deviations between measurement results and numerical results. He found that a Manning coefficient equal to $0.022 s/m^{1/3}$ showed a better fit between the measurements and the numerical model. Possibilities for such a poor fit with a Manning coefficient of $0.026\, s/m^{1/3}$ might be related to a bias in the measured discharge, an excessively large wall friction or the amount of diffusion of momentum, Chavarrías (2022). However, given the available data, Chavarrías (2022) stated that varying the Manning coefficient to improve the fit was the most reasonable solution. Figure 2.10 shows the relation between the measured and modelled water level gradient with an improved Manning coefficient equal to $0.022\, s/m^{1/3}$.

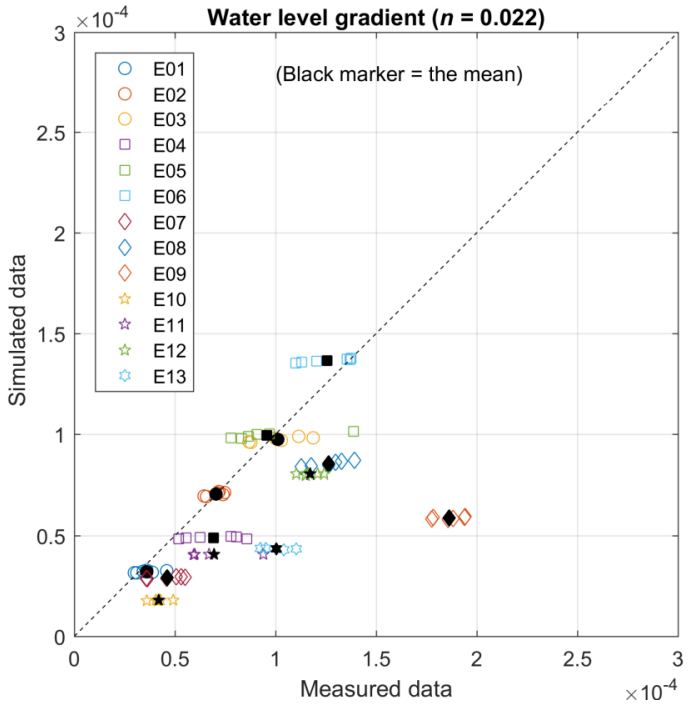

Figure 2.10: Relation between the measured and modelled water level gradient. The Manning coefficient in this plot is equal to $0.022\ s/m^{1/3}$. The labels E01 until E13 denote the hydraulic conditions used for the measurements for the reference situation without groynes (See Harms (2021) for more information). Source: Chavarrías (2022).

Even though figure 2.10 shows that there is a relation between the measured and modelled results, the difference is still significant for at least eight out of thirteen measurements. This difference can be up to a factor of three for the most extreme case. This complements the problem Limerinos (1970) described. He stated that it has always been difficult to accurately measure the bed roughness or bed friction of an open channel. Based on historical research, he concluded that there are inconsistencies between the existing relations for the bed friction. Among other things, he allocated these inconsistencies to the absence of sufficient amounts of field data.

2.5.3 Boundary conditions

When using a numerical model to simulate the flow in an open channel, one usually imposes a boundary condition at either end of the grid. A flow discharge is often used as an upstream boundary and a water level is often chosen for the downstream boundary.

Again, the measurements of Harms (2021) and numerical calibration of Chavarrías (2022) is used as an example. In his numerical model, Chavarrías (2022) uses a numerical grid that covers the entire surface area of the flume. Harms (2021) also tried to cover the entire area of the flume with the measurements. Obviously, it is impossible to locate measurement equipment exactly at the boundaries of the flume.

Modelling the entire flume is desirable as this can give the best insight in how the flow develops over the length of the flume. However, this might also cause problems for the numerical model.

Consider the actual flume with dimensions of $5 \times 40\,m$. At the upstream boundary, water flows into the flume with a constant discharge set by the pump. Reliable measurements regarding the characteristics of flow over and around submerged groynes can only be done once the flow has fully adapted to the flume bed. This occurs when the three-dimensional flow profile shows no significant variations between consecutive groyne fields, i.e. when the influence of the up- and downstream boundary is as small as possible, preferably negligible. To make sure the flow adapts as quickly as possible, a special inflow structure is created at the upstream boundary. See also section 3.1.

When modelling the entire flume, the model has to account for this adaptation process. This comes on top of the complex three-dimensional flow over and around the groynes. Modelling this complex flow has proven to be difficult enough on its own, as Van Schijndel & Jagers (2001), van Broekhoven (2007), Kruijt (2013), and Ambagts (2019) have already proven. Also having to account for the adaptation process of the flow might unnecessarily complicate the modelling.

A length of $40\ m$ might not be sufficient to completely eliminate the effects of the boundary conditions along a substantial part of the flume, so it might be preferable to seek a compromise in the area used in the numerical model. Instead of modelling the entire flume (from $x = 0\,m$ to $x = 40\,m$), one can choose to start the model at $x = 15\ m$ for example. The measurement equipment is able to measure the flow at exactly $x = 15\ m$, which it was unable to do at $x = 0\ m$. Reducing the size of the numerical grid will also have a positive effect on the modelling duration.

3 | Research methodology

In correspondence with the research objective and goals mentioned in section 1.2, a scaled physical model experiment is set up. For the experiment, the same measurements are done for the situation with reference groynes and the situation with streamlined groynes. This chapter elaborates on the research methodology used to achieve the research objective and goals. The figures in this chapter only show the geometry of the reference groynes.

3.1 Experimental model set-up

Figures 3.1 and 3.2 give an illustrative overview of the model set-up. The experiment is carried out in a flume with dimensions of $5 \times 40\ m^2$ where a river section is constructed with geometric scaling of $1:30$. This river section represents a part of a cross-section comparable to the river Waal, containing part of the main channel, six groynes, five groyne fields and a part of the floodplains, as stated in chapter 1.

To ensure hydraulically rough conditions, the entire flume bed is lined with gravel with a D_{n50} of 8 mm. As this experiment only focuses on the hydraulic conditions, the gravel is plastered onto the river bed with tile adhesive to prohibit any form of sediment transport. The groynes consist, just like the rest of the river bed, of a wooden frame plastered with tile adhesive and gravel. Once all the measurements with the reference groynes are finished, the streamlined groynes are installed with a downstream slope of 1:8. This means that the river bed is opened up to allow for new wooden frames to be installed and plastered with tile adhesive and gravel. Once completed, the second series of measurement runs are conducted.

The hydraulic conditions in the model are determined by an upstream and a downstream boundary condition. The upstream boundary condition is given by the inflow discharge. The inflow discharge is set by a 55 kW pump with a maximum outflow capacity of 400 l/s. The downstream boundary condition is given by the downstream water level, which can be adjusted via an adjustable water overflow. A water inlet serves the purpose of replenishing the water that exits the system via the overflow.

It is necessary for the upstream and downstream boundaries to have as little influence on the flow as possible. In order to minimize the effect of the upstream boundary, a special inflow structure is constructed with the goal of inducing as little inflow turbulence as possible. This way, the flow adapts to normalised conditions as quickly as possible.

Most of the measurement devices, signal converters, receivers and the computer are placed on top of a rolling platform above the flume. This rolling platform is positioned on tracks and moves in the flow direction, making it possible to easily measure along multiple transects.

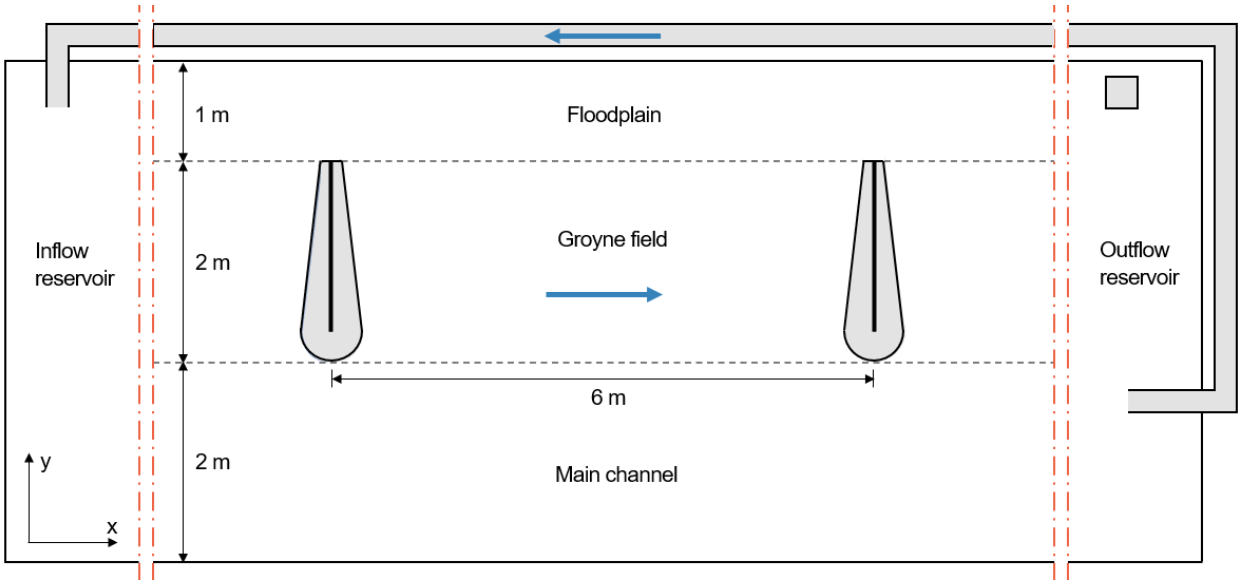

Figure 3.1: Overview of the experiment set-up. For clarity, this image shows just one groyne field. Initially, both the upstream and downstream slope of the groynes have a steepness of 1:3. For the streamlined tests, the downstream slope is adjusted to 1:8. The groynes have a crest width of 3 cm, a minimum crest height of 3 cm at the floodplain-groyne field border and a maximum crest height of 10 cm at the groyne field-main channel border. The groyne field has an upward facing slope of 1:25 in y-direction. The grey area connecting the outflow reservoir with the inflow reservoir is used for the return flow. This figure shows a top view of the model set-up.

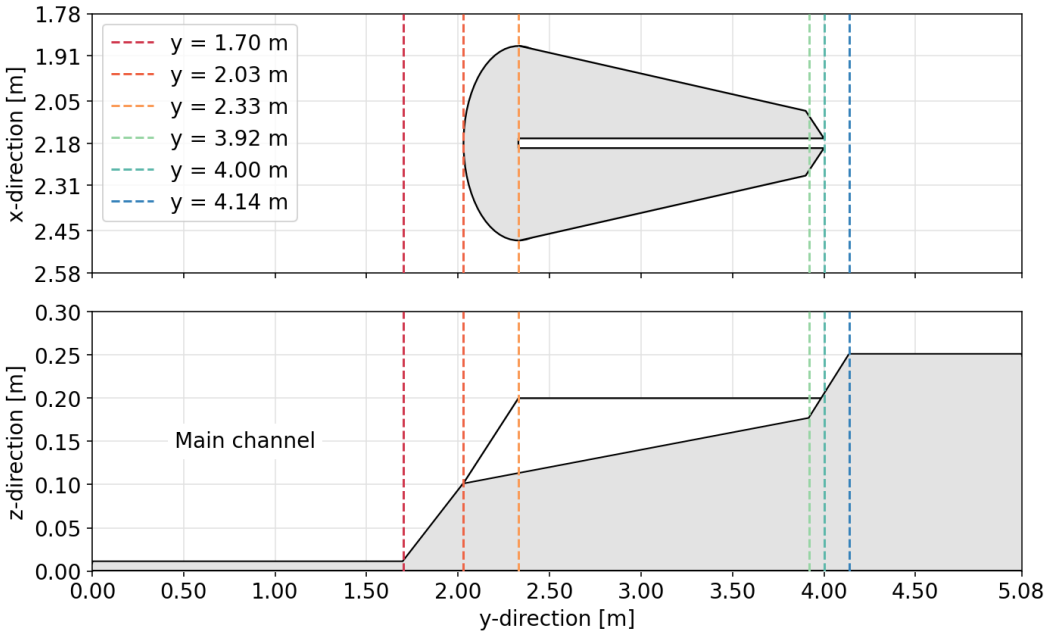

Figure 3.2: Dimensions of the experimental model set-up. All these distances were measured along multiple transects and have a margin of error of $\pm$ 0.005 m. For clarity, this figure only shows the dimensions for the reference groynes. Note that the width of the flume is equal to 5.08 $\pm$ 0.005 m.

3.2 Hydraulic conditions

For this experiment, each measurement run uses distinct hydraulic conditions. The hydraulic conditions are determined by the discharge and the downstream water level. Varying the hydraulic conditions for each measurement run allows a better data coverage, and subsequently, a better understanding regarding the flow around the groyne tip. This helps discovering patterns embedded in the raw data and improves the quality of the conclusions. Table 3.1 gives an overview of the distinct combinations of hydraulic conditions used for this experiment.

Table 3.1: Overview of the combinations of hydraulic conditions.

	Upstream discharge, Q (m^3/s)	**Downstream water level, h** (m)	**Groyne type**	**Measurement type**
1	0.23 $\pm$ 0.002	0.296 - 0.299	reference	Water level
2	0.25 $\pm$ 0.002	0.296 - 0.299	reference	Water level / flow velocity
3	0.27 $\pm$ 0.002	0.296 - 0.299	reference	Water level
4	0.29 $\pm$ 0.002	0.296 - 0.299	reference	Water level / flow velocity
5	0.23 $\pm$ 0.002	0.296 - 0.299	Streamlined	Water level
6	0.25 $\pm$ 0.002	0.296 - 0.299	Streamlined	Water level / flow velocity
7	0.27 $\pm$ 0.002	0.296 - 0.299	Streamlined	Water level
8	0.29 $\pm$ 0.002	0.296 - 0.299	Streamlined	Water level / flow velocity

The reason the discharge is susceptible to small fluctuations is because the pump can only be set up to output a constant amount of power. Due to small variations in water pressure, this constant power will result in small fluctuations in the discharge.

A discharge meter is used to determine the exact discharge through the outflow pipe and the power of the pump is set accordingly. Important parameters to consider when choosing a discharge are the Reynolds number (Re) and the Froude number (Fr). The Reynolds number should always be high enough to ensure fully turbulent flow ($Re > 3000$) and the Froude number has to be sufficiently small to ensure subcritical conditions ($Fr < 1$). The smallest Reynolds numbers are expected to occur near the floodplain in situations 1 and 5 from table 3.1. Based on measurements from Harms (2021), comparable hydraulic conditions result in a Reynolds number of around 9000. This is sufficiently higher than the laminar-turbulent threshold. The highest Froude numbers are expected to occur near the groyne crest. The combination of a low water depth and high flow velocities will result in the most extreme flow conditions. The measurements verified the maximum Froude number in the flume to be around 0.3.

While in theory the flow only becomes supercritical when $Fr > 1$, the flow in the flume starts to show flow phenomena that are incomparable to the Dutch river system when $Fr > 0.5$. To be on the safe side of the spectrum, it is desirable to keep the Froude number below 0.3.

One of the main research objectives is to quantify the effect of streamlining groynes in a river under fully submerged conditions during an extreme discharge event. The downstream water level in the flume is set at around 0.3 m. Considering the research objective, one might be inclined to choose a larger downstream water depth to better represent the extreme conditions. However, for the sake of measurement reliability it is desirable to manipulate the hydraulic conditions in the flume in such a way that the difference between

results of the situations with reference and streamlined groynes is as large as possible while remaining comparable to the Dutch river system. This reduces the chance that the results lie within the margin of error of the measurement equipment. If the results lie within the margin of error of the measurement equipment, this compromises the usability of the data.

An example of this phenomenon is given by the water level measurements from Harms (2021). Figure 3.3 shows the difference in water level slope between a situation with and without groynes for three different combinations of hydraulic conditions.

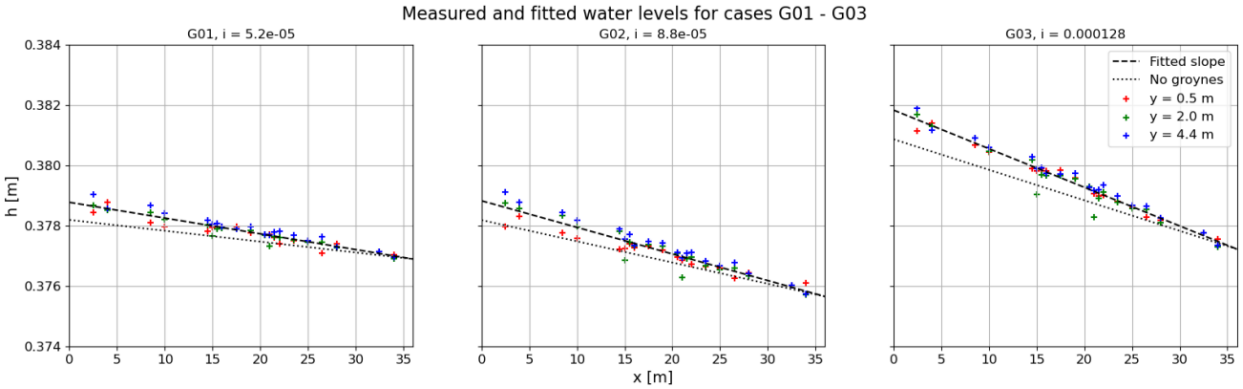

Figure 3.3: Measured water levels for three combinations of hydraulic conditions. In this figure, G01, G02 and G03 represent the hydraulic conditions under which the measurements were conducted. The water depth for all three situations is equal to 0.38 m and the discharge for G01, G02 and G03 is 0.174, 0.255 and 0.284 m^3/s respectively. Source: Harms (2021).

From figure 3.3 it is concluded that a higher discharge, i.e. more extreme hydraulic conditions, will increase the difference in water level slope between the situation with and without groynes. An increase in water level slope is related to an increase in overall resistance in the flume given a constant discharge, i.e. groynes add resistance. For this research, situations with reference and streamlined groynes are compared. It is expected that the induced resistance from streamlined groynes will be somewhere between the resistance of no groynes and the resistance of reference groynes. In other words, the measured water level slopes resulting from reference and streamlined groynes might lie within the margin of error of the measurement equipment while using the same hydraulic conditions as Harms (2021). For this reason, a smaller water depth and higher discharges are used.

An other argument that might be in favor of a smaller water depth is that according to Kruijt (2013), the lateral exchange of time-averaged streamwise momentum between the groyne field and the main channel increases for a smaller water depth. This means that the flow around the groyne tip intensifies compared to a situation with a larger water depth which makes for more optimal measurement conditions.

As stated in section 3.1, the downstream water level is controlled by an adjustable water overflow structure. Before starting the measurements, this water overflow structure was set to a constant level, such that the top of the structure is equal to a main channel water depth of just under 0.3 m. To get to a water depth of 0.3 m, a constant water overflow over the structure is required. Regardless of the flow conditions in the flume, the downstream water depth is constant when the inflow is equal to the outflow. In other words, the downstream water depth is controlled by adjusting the amount of water through the inlet. The constant overflow is observed by eye. Even though this is both a somewhat quantitative and a time consuming process, it turned out to be the most accurate method of imposing the downstream water depth. This is because a small variation in the water depth would result in significant changes in the overflow profile. Given the model set-up, it is not possible to quantify the accuracy of this method. However, based on experience, the margin of error of this method is qualitatively estimated to be in the order of 10^{-3} m.

3.3 Measurement techniques

This experiment makes use of two different measurement techniques. The first is to measure the water level using laser altimeters and the second is to measure the flow velocity using electromagnetic flow meters (EMF). These techniques and their respective details are described in this section.

3.3.1 Flow velocity

Electromagnetic flow meters (EMF) are used to measure the flow velocity. The measurement principle of an EMF is based on a conductive fluid moving through a magnetic field and it measures water velocities in two perpendicular directions (Deltares, 2020). The EMF meters are suspended from the platform with custom fixture plates. A friction-based rail system allows the EMF meters to be placed on a certain y-coordinate while a winch mechanism allows for positioning in z-direction. The accuracy of EMF positioning in x-, y- and z-direction is in the order of 10^{-3} m. The EMF meters are able to measure the flow velocity in both x- and y-direction with a maximum of 2.5 m/s and an accuracy of $\pm$ 0.01 $m/s \pm 1$ % of the measured value (Deltares, 2020).

The velocity output of the EMF meters is given in volts (V). The following formula is used to convert the output signal to m/s. This formula is the result from calibrations of the EMF meters by the manufacturer. In this formula U is in m/s and V is in volts.

$$U = -0.000188 \cdot V^2 + 0.1023 \cdot V + 0.002 \tag{3.1}$$

Before each measurement run, the EMF meters are calibrated for a situation without flow. The meters are calibrated once the displayed output values fluctuate within 0.1 V from 0. During initial testing it was observed that the EMF meters are very sensitive to variations in z-direction when they are placed close together in y-direction. Therefore, every time the z-coordinates of the EMF meters change, they are recalibrated. This is a time consuming process (as the flow velocities in the flume have get back to 0, which takes up to 30 minutes every time) but absolutely necessary if one wants to gather accurate data. This effect is less present when the EMF meters are spaced further apart. Every measurement run is concluded with a zero measurement. This is to check how much each individual EMF meter deviates from its calibration before the measurement run. Based on this data, the measured flow velocity error after each measurement run turned out to be structurally below 10^{-2} m/s, a few exceptions aside.

3.3.2 Water level

Laser altimeters are used for the water level measurements. These laser altimeters measure the round-trip time of a light pulse between emission and the returned surface reflection to determine the distance. The measured distance is depicted as a deviation from a calibrated reference level. The output values for the laser altimeters are between 2 and 10 V and the devices are calibrated such that this equates to a vertical distance of 40 mm. The laser altimeters used during this experiment need a solid and non transparent surface to reflect the laser beam on. It took many iterations to make an object that was both flexible enough to follow the small water level changes and strong enough to stay emerged above the water at all times. These object were adhered to the laser fixture plate so that it would always be in the same position relative to the laser.

The laser altimeters are able to measure a distance with an accuracy in the order of 10^{-6} m (Micro-Epsilon, 2008). It is expected that the difference between two consecutive water level measurement points will be in the order of 10^{-4} m. So the difference between two measurement points might, in some cases, be smaller than the accuracy of the upstream and downstream boundary conditions. Therefore, the decision was made to conduct all water level measurements in one single measurement run. This guarantees that the hydraulic conditions remain as constant as possible throughout the measurement run, which significantly reduces the problem described above. Obviously, a separate measurement run was necessary for the streamlined groynes. To keep the uncertainties imposed by the hydraulic conditions as small as possible between these two runs, extra care was given to imposing the downstream water level, as well as to the positions of the laser altimeters relative to the platform. To mitigate as many instabilities in the set-up as possible, the laser altimeters are mounted to the platform as rigidly as possible.

A couple of zero measurements are done to quantify any irregularities in the rails supporting the platform. For these measurements, the flow velocity in the flume is zero and the laser altimeters use a special distance wheel to measure at a constant distance interval instead of a constant time interval. The expected error of this deflection is expected to be in the order of 10^{-3} m in vertical direction as the rail was professionally aligned. This is larger than the expected difference between two measurement points, which is why these zero measurements are necessary. Figure 3.4 shows an image of an EMF meter and a laser altimeter. The overall accuracy of the water level measurements is expected to be in the order of 10^{-4} m.

Figure 3.4: Image of an EMF probe (left) and a laser altimeter (right).

3.4 Measurement duration

When choosing a measurement duration, two basic principles hold: a longer duration gives more reliable results and a shorter duration will shorten the experiment duration. Finding the optimal combination of reliability and time-efficiency will lead to the right measurement duration for the used equipment. The optimal measurement time is not a single value, but rather a range in which the optimal combination holds true. It is up to the experimental researcher to determine the exact measurement duration within this range.

A duration of five minutes is used for the flow velocity measurements and a duration of one minute for the water level measurements. These decisions are based on a couple of long-duration measurements of which the results are displayed in figures 3.5 and 3.6. These figures show that for both the flow velocity measurements and the water level measurements the deviation from the average is less than 0.5 % of

the long-duration average. More of these long-duration measurements were done and all show a similar result. Longer measurement duration would only improve the reliability by a negligible amount. To be on the safe side, a shorter measurement duration is not used, this is also substantiated by the fact that both Harms (2021) and Yossef (2004) use a duration of five minutes for similar set-ups.

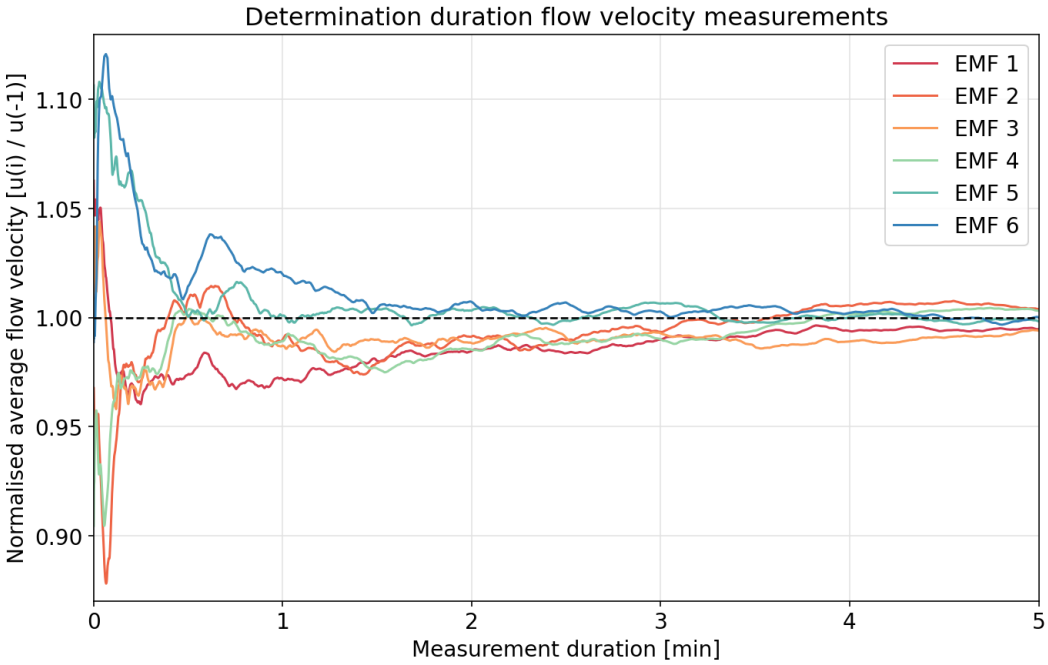

Figure 3.5: This figure displays the normalised average flow velocity in x-direction after every data point in a long-duration measurement. The total duration of this measurement was 25 minutes. For figure clarity, only the first five minutes are displayed here.

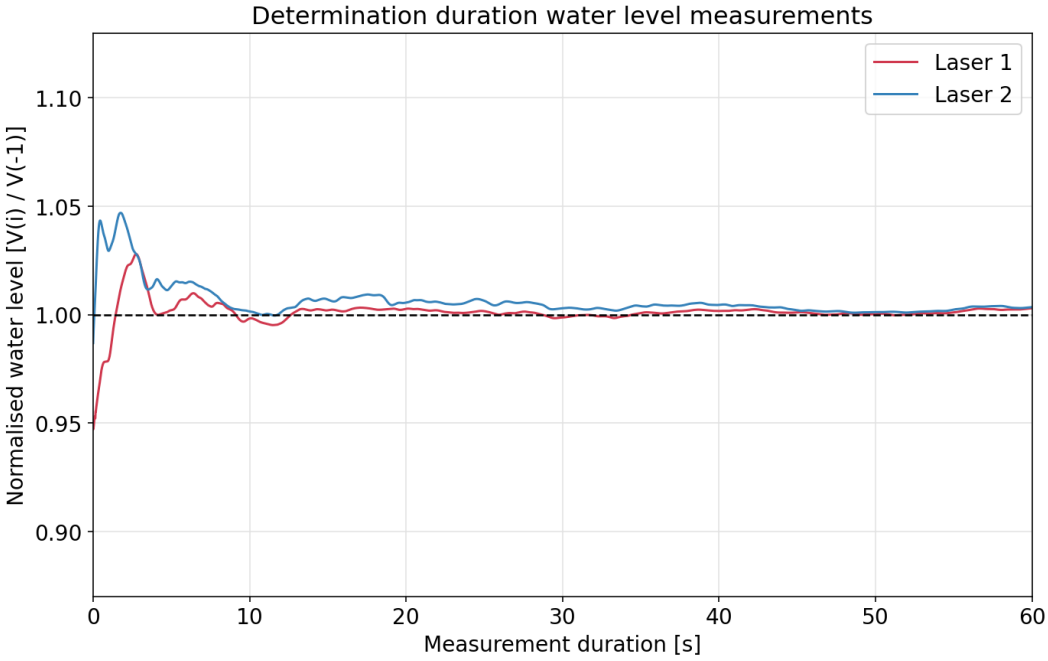

Figure 3.6: This figure displays the normalised water level after every data point in a long-duration measurement. The total duration of this measurement was five minutes. For figure clarity, only the first minute is displayed here.

3.5 Measurement locations

The measurements for this experiment are divided into three categories. The first type of measurements is concentrated around the groyne tip. These measurements are used to get better insight in the flow processes around the groyne tip and consist of detailed flow velocity measurements. From now on, these measurements are referred to as the "groyne tip measurements" and use the EMF meters described in subsection 3.3.1.

The second type of measurement is related to the numerical modelling of the problem. For numerical modelling it is important that the entire flume can be replicated numerically. This means that next to the detailed measurements, multiple transacts of measurements along the length of the flume are taken. After the situation in the flume is modelled successfully, the numerical model is able to scale up these results to use for real life applications. These measurements are referred to as the "flume measurements".

The third measurement type uses the laser altimeters to measure the water level in the flume. These measurements will give insight in the evolution of the water level over the length of the flume at different point along a transact. They are also used together with the flow velocity measurements to calculate the specific discharge for each measurement point. The locations for the water level measurements are also located in figures 3.7 and 3.8.

Every measurement point has a unique (x, y, z) coordinate with respect to the origin point. This origin point is represented by O $(0, 0, 0)$ as depicted in figure 3.8. The groynes are labelled A up until F.

3.5.1 Groyne tip measurements

The groyne tip measurements are focused around groyne *C* and *D*, because the flow is expected to experience the least amount of influence from the boundary conditions in this region of the flume. The aim of the groyne tip measurements is to acquire as much data of the flow around the groyne tip as possible. Therefore, the density of the measurements is as high as the measurement equipment allows while still satisfying the time constraints of the experiment.

To capture the complex flow around the groyne tip, six EMF meters are positioned close to each other along each transact. Test measurements and data from the EMF manufacturer are meant to give insight in the distance multiple EMF meters can be located from each other without obstructing their magnetic fields. This in turn compromises the measured data.

Results from test measurements in the flume without flow found that two EMF meters start to interfere with each other when spaced less than 70 mm apart. The manufacturer of the meters states that the probe of the EMF should be at least 30 mm above the bed and below the water surface for a reliable signal (Deltares, 2020). This means the electromagnetic field of the EMF can be approximated by a circle with a radius of 30 mm. This means that two EMF meters should be separated by at least 60 mm. This research uses a minimum distance between two EMF meters of 100 mm, as this is as close as the measurement set-up would allow.

In figure 3.7, the EMF locations are depicted by the blue circles. The groyne tip measurements are repeated for hydraulic conditions 2, 4, 6 and 8 from table 3.1.

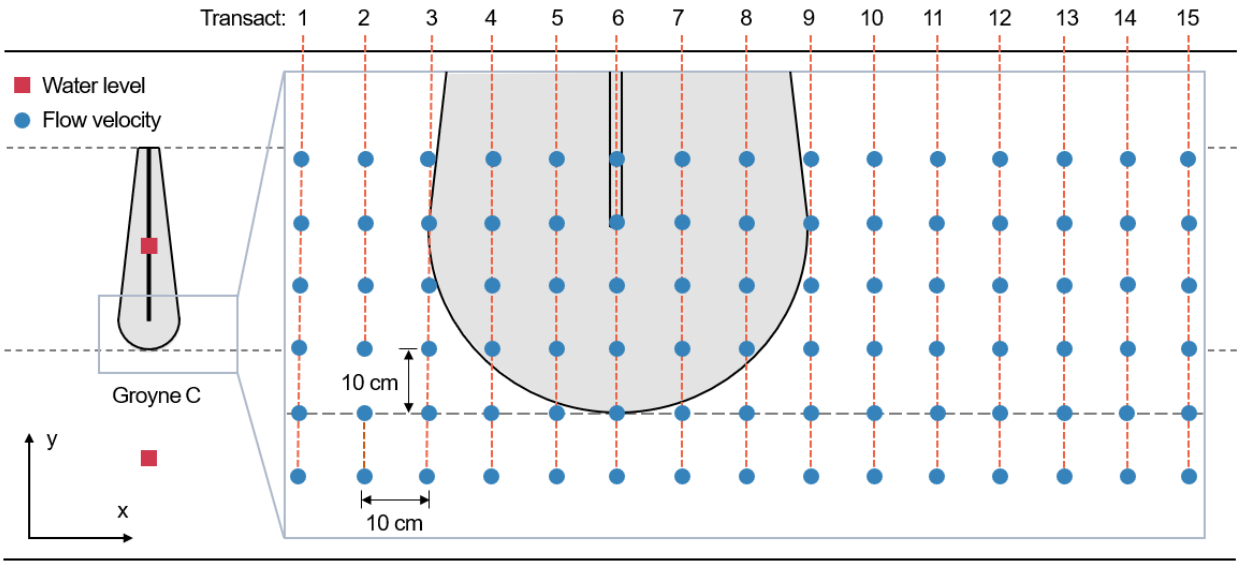

Figure 3.7: Overview of the measurement locations for the groyne tip measurements. Along each transact, the flow velocity measurements are repeated for multiple fractions of the water depth. Namely: 20, 40, 60 and 80 % of the local water depth. The blue dots that correspond to the velocity measurements form a grid in which the points are spaced 100 mm apart in both x- and y-direction. This figure displays groyne C with its corresponding transacts 1 to 15. The same measurement locations apply for groyne D, measuring along transacts 16 to 30.

3.5.2 Flume measurements

The flume measurements give a sufficient data coverage over the length and width of the flume. Figure 3.8 provides an illustrative overview of the measurement locations of the EMF meters. The transacts along which the flow velocity is measured are equally distributed over the length of the flume. The flow velocity measurements cover the entire width of the flume, except for the floodplain, where the shallow water depth of only 50 mm does not allow for the use of an EMF meter. To obtain sufficient data coverage over the width of the flume, each transact is measured at twelve measurement points in the y-direction. However, since only six EMF meters are available for this experiment, each transact is measured twice, given a constant z-coordinate of the EMF probes.

The flume measurements are repeated for hydraulic conditions 2, 4, 6 and 8 from table 3.1.

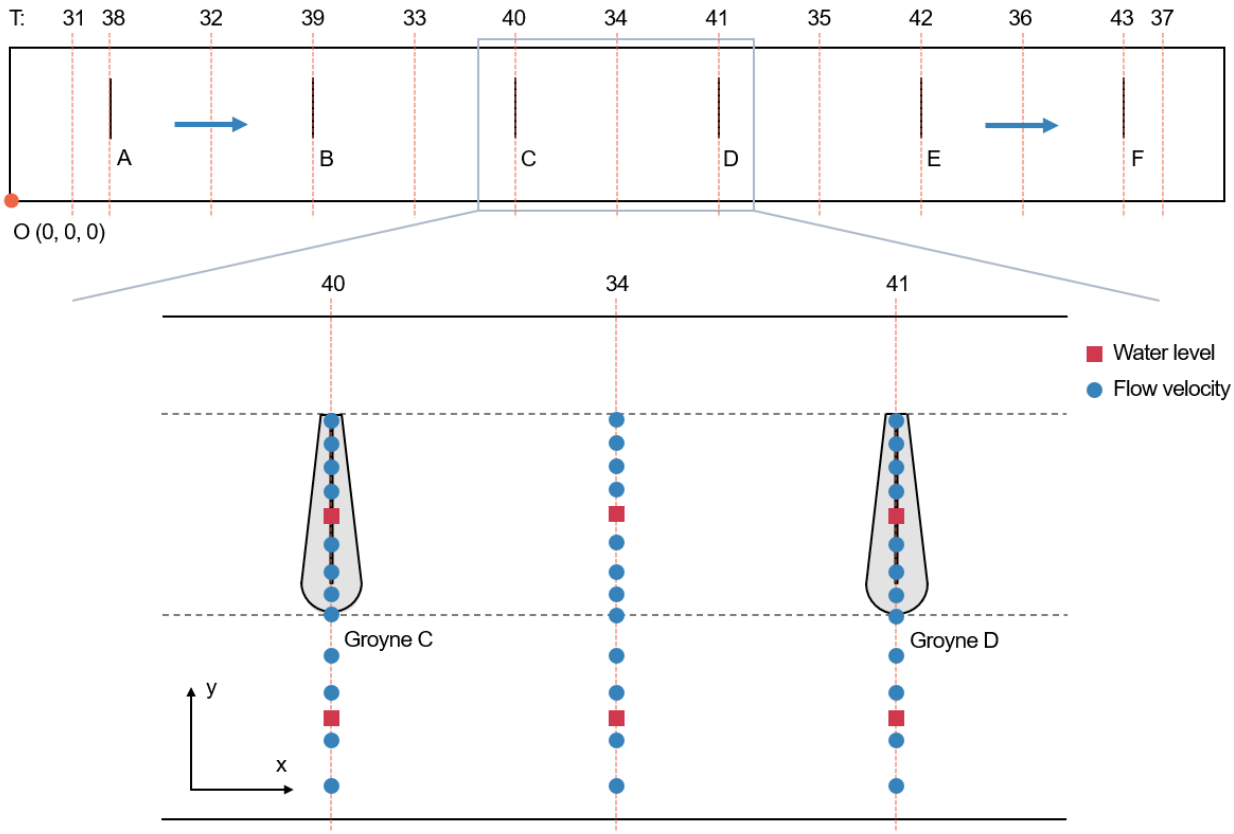

Figure 3.8: Overview of the measurement locations for flume measurements. Just as for the groyne tip measurements, the flow velocity is measured for multiple fractions of the water depth. In this case: 40, 60 and 80% of the water depth. The flow velocity measurements represented by the blue dots are distributed over the entire width of the flume with the exception of the floodplain. The water level measurements represented by the red squares have the same location in y-direction as for the groyne tip measurements.

4 | Results water level measurements

Chapter 3 shows that this experiment makes use of two measurement techniques: laser altimeters for the water levels and EMF meters for the flow velocities. This chapter presents the results from the water level measurements described in subsection 3.3.2.

4.1 Processing the water level data

This section describes the process necessary to transform the raw data into usable water levels. To plot the actual water level, the raw data undergoes a couple of translations and modifications. The raw data of the laser altimeters is given in V. To translate the data from V to m/s, the used calibration settings are used: the output range of 8 V (from 2 to 10 V, as stated in subsection 3.3.2) translates to a vertical distance of 40 mm. Using the known downstream water level, these values can now be translated to actual water levels. The last step is to correct for the irregularities from the rails supporting the platform. Figure A.2 in appendix 7.2 is a visualisation of these irregularities in the rails. Figure 4.1 shows the final result of the water level measurement run with streamlined groynes and a discharge of 0.29 m^3/s. To enhance the visual consistency of figures 4.1 and the figures in appendix 7.2, the x-axis of these figures align and the scale of the y-axis is the same.

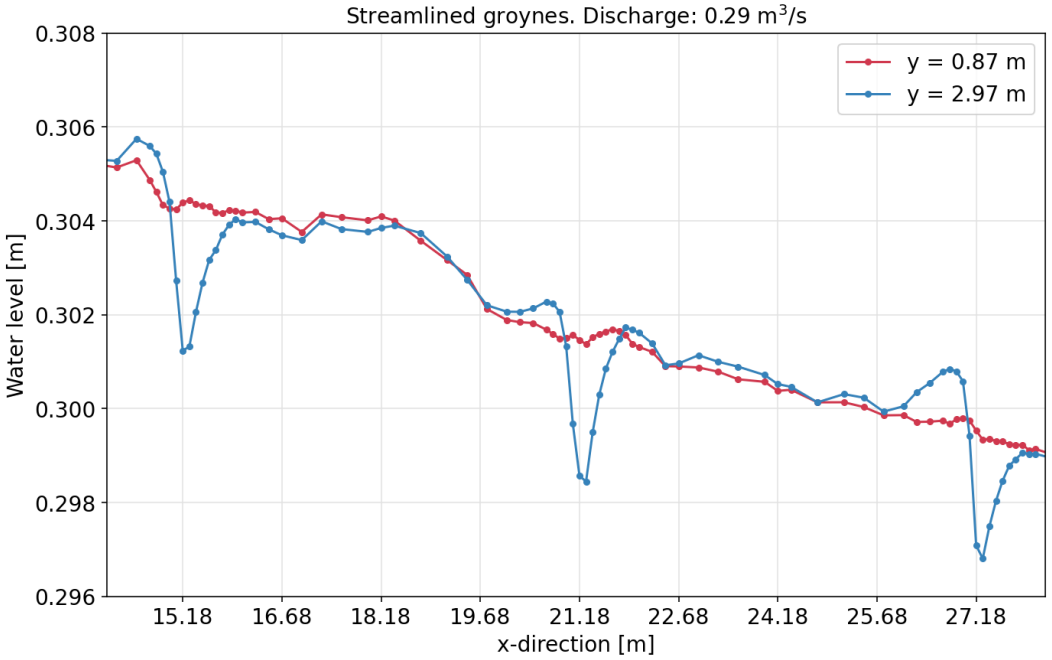

Figure 4.1: Final result of one water level measurement run. The figure covers groynes C, D, and E (see figure 3.8) as this region has the highest measurement density. Every dot represents one water level measurement. The x-coordinates are x = 15.18 m, x = 21.18 m, x = 27.18 m for the crests of groyne C, D and E respectively. The red line shows the measurements in the main channel and the blue line represents the measurements in the groyne fields.

Appendix 7.2 shows the figures of the water levels for the other discharges for both the reference and streamlined groynes. The results throughout these figures are consistent and do not show any inexplicable phenomena, which benefits the comparability. For this research, only two laser altimeters were available. The way the measurements were set-up (subsection 3.3.2) made it impossible to measure more points along a transact with the same level of accuracy and applicability. Appendix 7.2 gives an illustrated example of this phenomenon.

4.2 Results

The most obvious result from the water level measurements from figure 4.1 is the visualisation of the effect that the groynes have on the water level. The water level in the main channel stays relatively undisturbed while the water level shows a clear drop at the locations of the groynes. Throughout the various measurement runs, the results are comparable and show consistency, as stated in section 4.1. This is likely because of all the effort that went into optimising the accuracy of these measurements. Figure 4.2 gives a detailed overview of the flow over groyne D at x $= 21\ m$ for discharges of 0.25 and 0.29 m^3/s.

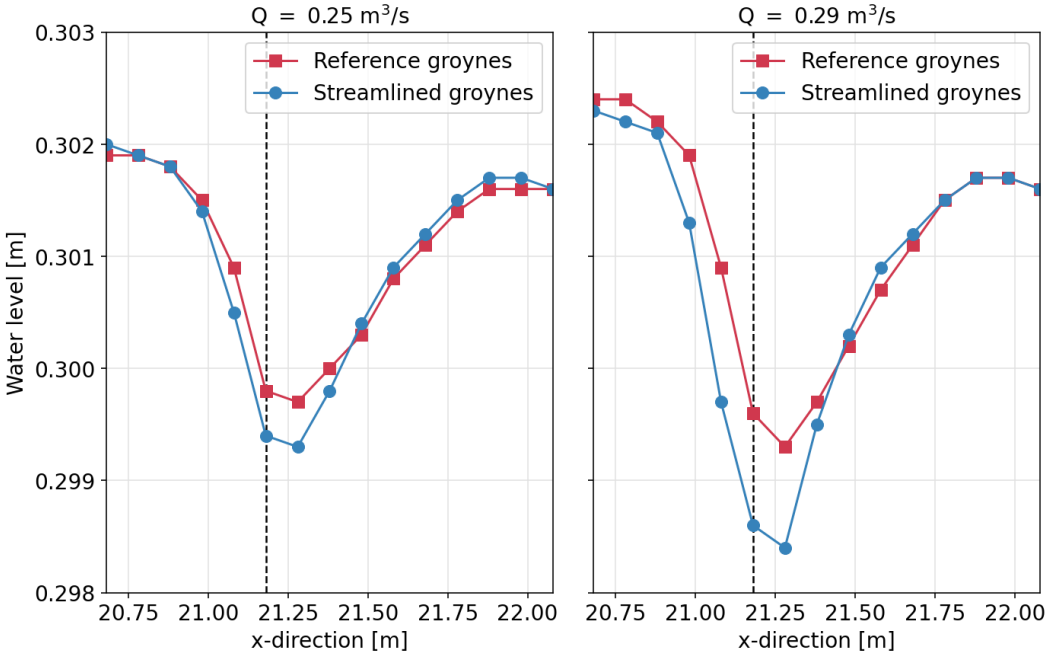

Figure 4.2: Detailed overview of flow over groyne D at x $= 21\ m$. The vertical line represents the groyne crest. Note that the value of the last measurement point is the same for all four graphs. This is to increase the comparability of the graphs and it does not represent the actual water level at this measurement point.

In figure 4.1, the rapid change in water level can be ascribed to the flow contraction and divergence as a result of acceleration and deceleration of the flow. The steepness of the slope of the water level is related to the acceleration of the flow and the absolute change in water level is related to the actual flow velocity. This would suggest that streamlined groynes should experience larger flow velocities near the crest compared to reference groynes, assuming the flow conditions in front of the groynes are somewhat comparable for the reference and streamlined groynes. See also chapter 5 where the flow velocity data is analysed.

It is interesting to note that at the first measurement point after the groyne crest, i.e. 10 cm after the groyne crest, the water level remains somewhat constant. This means the deceleration of the flow starts somewhere between 10 and 20 cm away from the groyne crest. Furthermore, there is a small rise in water

level in front of the groyne. This induces a transverse water level slope that is partially responsible for water flowing around the groyne as opposed to flowing over the crest of the groyne.

It is important to be aware of the scale of the y-axis of figure 4.1. The difference in water level between the groyne field and the groyne crest at y = 2.97 m is around 4 mm, or in the order of 10^{-3} m. The difference in bed level between the groyne field and the groyne crest at y = 2.97 m is around 6 cm, or in the order of 10^{-2} m, see figure 3.2. In other words, the bed level change is an order of magnitude larger than the water level change. This matters when looking at the specific discharge in section 5.2.

Figure 4.1 shows a local increase in water level between groyne C and D (between x = 17 m and x = 19.5 m) in both the main channel and the groyne field. This increase is not present between groyne D and E. Figure A.3 shows that this phenomenon is also present for a discharge of 250 l/s. Even though the reference groynes have less measurement points between groynes, it is still visible that this local increase in water level likely also occurs for the reference groynes. Note that the flow distance of the flume is around 34 m. This is likely insufficient to obtain an equilibrium flow. Therefore, minor differences in local water level profiles (and local water level profiles) are to be expected.

Table 4.1 shows the amount of water level measurements and the resulting water level slopes for the various hydraulic conditions for both the reference and the streamlined groynes. Table 4.1 presents two different columns which both contain water level slopes. The water level slopes in the fourth column are calculated between x = 6.18 m and x = 30.18 m (1). The water level slopes in the fifth column are calculated between x = 18.18 m and x = 30.18 m (2). For the reference groynes the measurement runs consisted of either 7 or 37 measurements each and for the streamlined groynes the measurement runs consisted of either 7 or 84 measurements each. Runs 3, 4, 7 and 8 have significantly more measurements than runs 1, 2, 5 and 6. This is because for runs 3, 4, 7 and 8 the water level data is also used in combination with the flow velocity data for the calculation of the specific discharge. Runs 1, 2, 5 and 6 are only used for water level measurements.

The reason runs 4 and 8 consist of 84 measurements and runs 3 and 7 of 37 measurements is the result of an insufficient data coverage for runs 3 and 7. For runs 3 and 7, the measurements were focused around groyne C and D, with no information on the water level in the groyne fields. Upon an initial data analysis at the time the flume was being modified for the streamlined groynes, it was decided to include extra water level measurements for the groyne fields between groyne C and D, between D and E and for groyne E. This was for measurement runs 4 and 8.

Table 4.1: Resulting main channel water level slopes.

	Upstream discharge, Q (m^3/s)	**Groyne type**	**No. measurement points**	**Water level slope (1)**	**Water level slope (2)**
1	0.23 ± 0.002	reference	7	$-1.919 \cdot 10^{-4}$	$-1.330 \cdot 10^{-4}$
2	0.23 ± 0.002	Streamlined	7	$-1.859 \cdot 10^{-4}$	$-1.240 \cdot 10^{-4}$
3	0.25 ± 0.002	reference	37	$-2.688 \cdot 10^{-4}$	$-2.076 \cdot 10^{-4}$
4	0.25 ± 0.002	Streamlined	84	$-2.547 \cdot 10^{-4}$	$-2.077 \cdot 10^{-4}$
5	0.27 ± 0.002	reference	7	$-3.041 \cdot 10^{-4}$	$-2.228 \cdot 10^{-4}$
6	0.27 ± 0.002	Streamlined	7	$-3.024 \cdot 10^{-4}$	$-2.261 \cdot 10^{-4}$

7	0.29 ± 0.002	reference	37	$-3.834 \cdot 10^{-4}$	$-2.978 \cdot 10^{-4}$
8	0.29 ± 0.002	Streamlined	84	$-3.694 \cdot 10^{-4}$	$-3.210 \cdot 10^{-4}$

The fourth column of table 4.1 shows a reduction in water level slope for the streamlined groynes when compared to the reference groynes for every discharge used during this experiment. This difference varies between 1 and 5 %. The fifth column of table 4.1 shows a reduction in water level slope for the lower discharges and a slight increase for the higher discharges.

It is difficult to determine a single representative value for the water level slope in th flume. Due to the limited length of the flume, it is possible that the flow does not reach equilibrium flow. This causes the average water level slope to change over the length of the flume. However, the last section of figure 4.1, from x $= 21\ m$ onward, does seem to indicate the presence of equilibrium flow.

The fourth column in table 4.1 may indicate a more favorable outcome, i.e. a decrease in water level slope regardless of the upstream discharge. However, the values from the fifth column may provide a more accurate representation of equilibrium flow. This is because the upstream boundary has the smallest influence in this region of the flume. It is important to be aware that the choice of the region between which the water level slope is calculated can influence the conclusions regarding the effect of streamlining groynes. In the case of this research, it is stated that the average influence of streamlining groynes on the water level slope is small.

5 | Results flow velocity measurements

This chapter presents the results from the flow velocity measurements as described in subsection 3.3.1. While the possibilities with just the water level measurements are limited, there are a lot more possibilities with the flow velocity measurements and the combination of flow velocity and water level.

5.1 depth-averaged flow velocity

For the flow velocity data to be usable, it first has to be converted from V to m/s using equation 3.1. Figures 3.7 and 3.8 give a visual overview of the measurement locations. For each (x, y) measurement point either three or four measurements in z-direction were conducted. This opens up the possibility to plot the vertical velocity profile at each (x, y) coordinate. Figure 5.1 shows two of these velocity profiles.

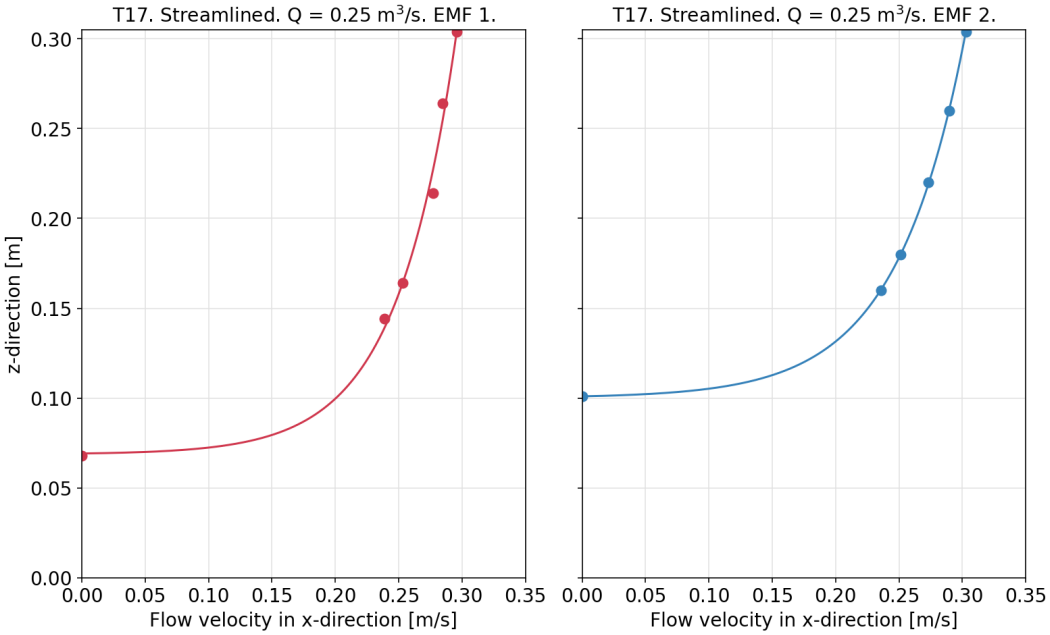

Figure 5.1: Plot of the flow velocity profile in z-direction for two EMF meters spaced 10 cm apart in y-direction under the same hydraulic conditions.

The first step to plotting the velocity profiles is to plot the measured flow velocities at the corresponding (x, y, z) coordinates. The flow velocity at the bed level is constantly set to 0 m/s. Now it is possible to fit a matching curve through this data and extrapolate this curve to the water surface. By integrating this curve fit over the water depth, it is possible to calculate the depth-averaged flow velocity, which is then multiplied by the water depth to get the specific discharge at the corresponding (x, y) coordinate.

To get a reasonably accurate estimation of the depth-averaged flow velocity, it is necessary to use the resulting curve fit as the basis for the depth integration. The curve fit method that is used tries to fit an exponential curve through the data points. This method works as long as the measured data somewhat resembles the known flow velocity profile for fully developed uniform flow.

Being able to calculate the depth-averaged flow velocities, it is possible to plot the the depth-averaged flow velocity over the width of the flume. Figure 5.2 shows the result of the calculation of the depth-averaged flow velocity profile over the width of the flume for one transact at a groyne crest. The measurement points are distributed between y $= 0.30\ m$ and y $= 3.83\ m$. In subsection 3.5.2 it was explained that due to limitations of the EMF meters, it was not possible to measure flow velocities in the floodplain. Note that in figure 5.2 and other transacts taken at the groyne crests, it is possible to combine the "groyne tip measurements" and the "flume measurements" (section 3.5), making for a total of fifteen data points along these specific transacts.

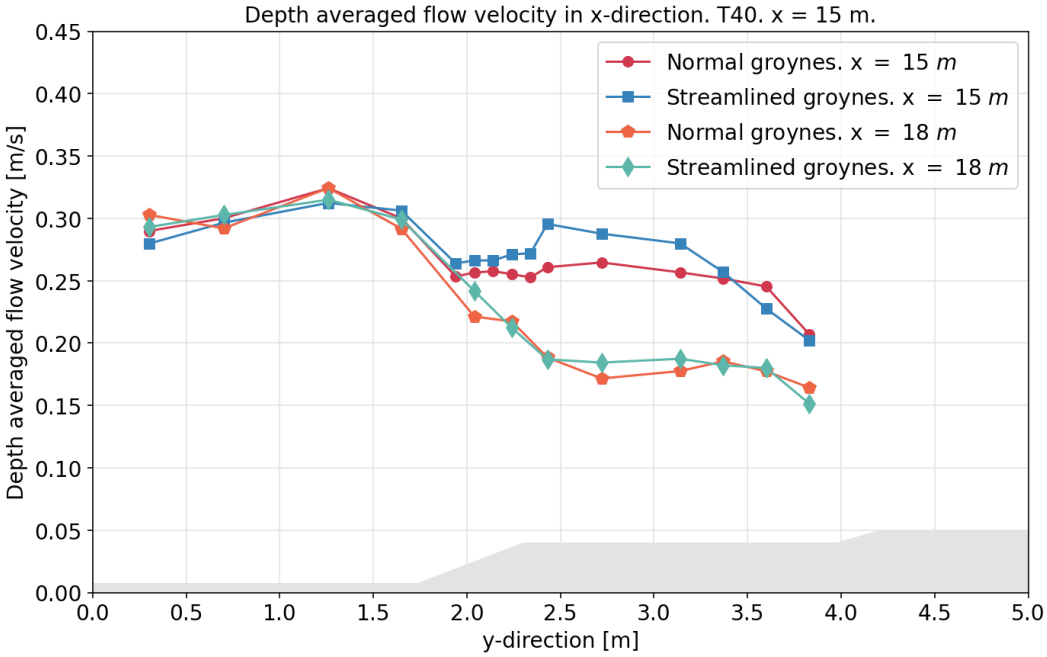

Figure 5.2: Plot of the depth-averaged flow velocity over the width of the flume at x $= 15\ m$ and x $= 18\ m$.

Figure 5.2 shows that streamlining the downstream slope of the groynes leads to higher flow velocities over the crest and the tip of the groynes compared to the situation with reference groynes. The relative difference is in the order of 5 %. This observation is consistent for groynes C, D, E and F. It is likely that the influence of the upstream boundary prohibits this flow pattern from occurring at groyne A and B. Closer to the floodplain, the results of streamlining is actually a decrease in flow velocity compared to a situation with reference groynes. Between two groynes, the depth-averaged flow velocities for the situations with reference and streamlined groynes do not show a significant difference.

These observations coincide with the water level data from chapter 4. Figure 4.1 shows that the water levels in the groyne fields are roughly the same for both the reference and streamlined groynes. However, the water level drop over the groynes is larger for the streamlined groynes compared to the reference groynes. This indicates higher flow velocities over the crests of the streamlined groynes and equal flow velocities in the groyne fields. These observations show consistency throughout both measurement techniques. Section 6.2 calculates the total discharge for each transact as an extra verification of the consistency and accuracy of the data.

5.2 Specific discharge

Combining the water level data from section 4.1 and the depth-averaged flow velocities calculated in section 5.1, it is possible to calculate the specific discharge at each (x, y) measurement point. Figure 5.3 shows the specific discharges for the same transact as figure 5.2.

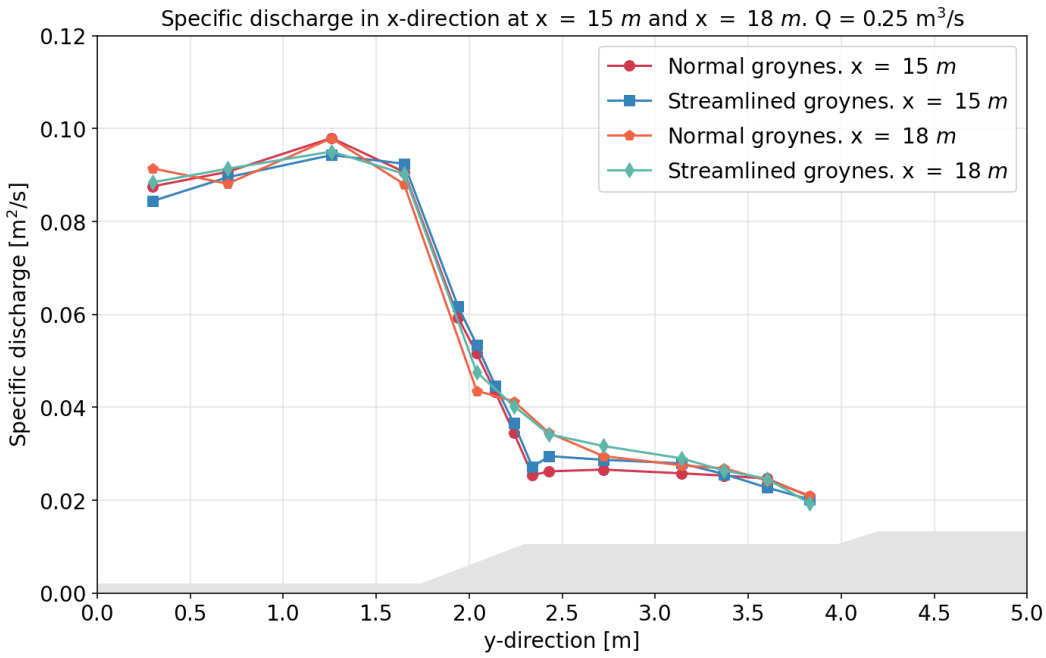

Figure 5.3: Specific discharge over the width of the flume at x $= 15\ m$ (groyne crest) and x $= 18\ m$ (groyne field).

The relative difference in specific discharge between the situation with reference and streamlined groynes is consistently slightly smaller than the difference in depth-averaged flow velocity, but still in the same order of magnitude. The reason the relative difference is slightly smaller for the specific discharge is because of the differences in water level over the crest of the groynes. As stated in section 4.2, the water level over the crests of the groynes is lower for the streamlined groynes, which coincides with the increase in depth-averaged flow velocity. At y $= 2.24\ m$, the gradient of the specific discharge changes rapidly at the groyne crest. This is not visible in the groyne field.

This redistribution of the discharge over the width of the flume is likely the reason why there is no clear difference in water level slope, as explained in chapter 4. Within the boundaries of this experiment, the effect of streamlining groynes does not express itself as a change in water level slope, but as a redistribution of the discharge between the main channel and the groyne field. In an experiment where a weir is tested over the entire width of the flume, the effect of streamlining would probably express itself as a change in water level slope under equal hydraulic conditions (as explained by Sieben (2003)).

5.3 Flow field around the groyne tip

Using the "groyne tip measurements" described in subsection 3.5.1, the effect of streamlining groynes is investigated on a more detailed level. First, a flow velocity and flow direction map from the flow around the groyne tip is made. Figures 5.4 and 5.5 show these maps for both the reference and streamlined groyne D with a discharge of 0.29 m^3/s.

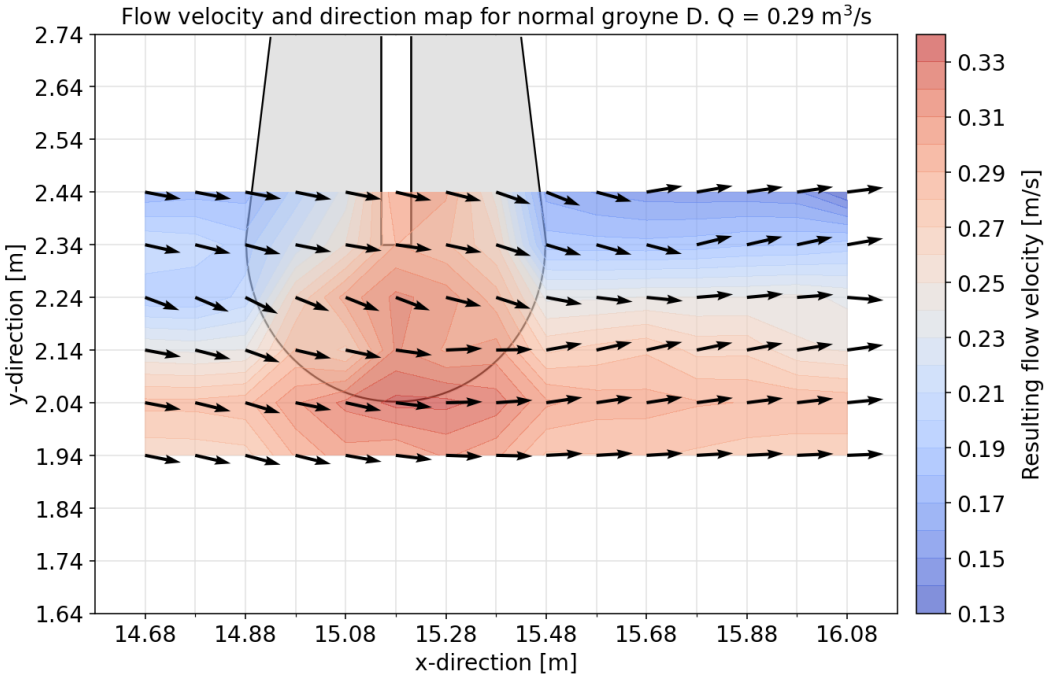

Figure 5.4: Flow velocity and direction map of reference groyne D for a discharge of 0.29 m^3/s. Each point corresponds to an (x, y) measurement point at which multiple flow velocity measurements are taken over the vertical. The arrows represent the depth-averaged flow direction and the colours represent the magnitude of the resulting depth-averaged flow velocity. Note that for figure clarity, the flow angles are multiplied by a factor of 3. The range of the color bar is equal for both figure 5.4 and 5.5.

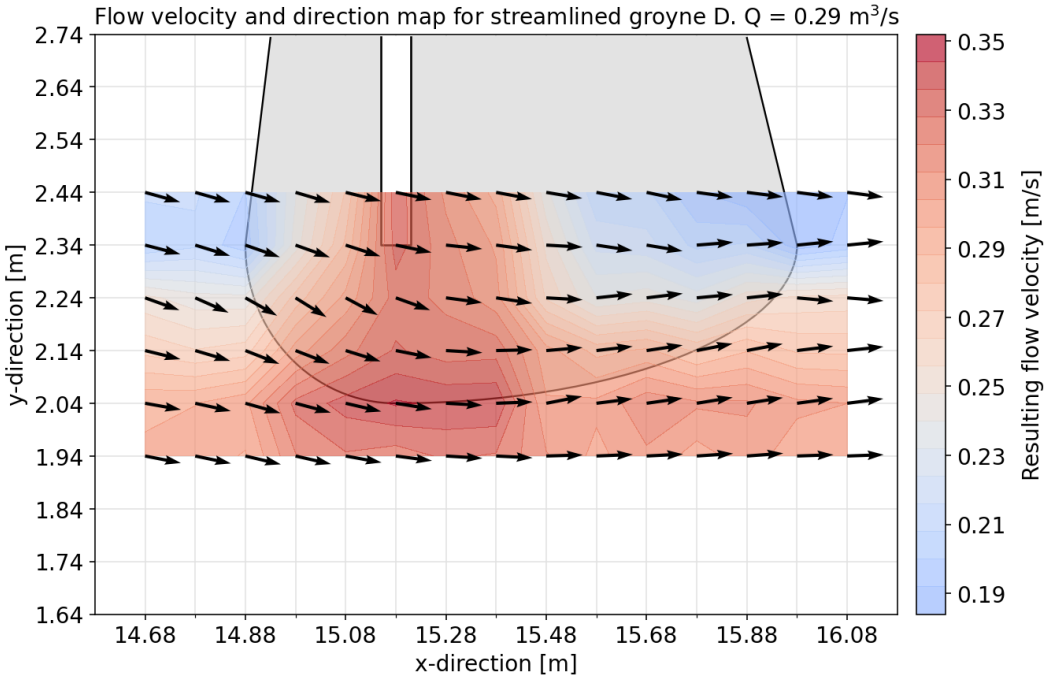

Figure 5.5: Flow velocity and direction map of streamlined groyne D for a discharge of 0.29 m^3/s.

Figures 5.4 and 5.5 show that the flow direction upstream of the groyne tip is already angled towards the main channel, consistent with the water level profiles. The groyne tip measurements start 20 cm upstream of the groyne. This indicates that the region of influence of the groyne reaches further upstream than the groyne tip measurements. This is also substantiated by figure 4.1, where the region of influence of the

groyne reaches to around 1 m upstream of the groyne. Also, the general flow velocity around the groyne tip is consistently larger for the streamlined groynes. For all situations, the highest flow velocity is found at y = 2.04 m at the location of the groyne crest. This is easy to explain: the flow upstream of the groyne pushes water toward the main channel, however, due to the consistent cross-section of the main channel, the natural flow direction in the main channel is in streamwise direction. This exerts at counter force which causes the flow direction of approach the streamwise direction which is responsible for the larger flow velocity at the location.

Remarkable is the rapid change in flow direction behind the reference groyne, which is not visible for the streamlined groyne. This difference is consistent for both groyne C and D and discharges 0.25 m^3/s and 0.29 m^3/s (so all the locations and conditions for which the groyne tip measurements from subsection 3.5.1 were carried out), even though this rapid change in flow direction has a smaller magnitude for groyne C. An explanation for this phenomenon is that this rapid change in flow direction is related to the rapid change in bed level and the resulting flow separation, which in turn might be responsible for some immeasurable 3D flow structure causing the flow to rapidly change direction.

5.4 Turbulence around the groyne tip

A more detailed analysis of the turbulence development around the groyne tip can explain the higher flow velocities and higher discharges over and around a streamlined groyne compared to a reference groyne.

First, the relative turbulence intensity (r) around the groyne tip is considered. The turbulence intensity is defined as the square root of the variance of a velocity component, and is also referred to as the mean amplitude of the velocity fluctuations (Uijttewaal, 2003). Formula 5.1 is used to calculate the relative turbulence intensity and the results are presented in figures 5.6 and 5.7.

$$r = \frac{\sqrt{\overline{(u-\overline{u})^2} + \overline{(v-\overline{v})^2}}}{\sqrt{\overline{u}^2 + \overline{v}^2}} \tag{5.1}$$

In which u is the flow velocity in streamwise direction and v the flow velocity in transverse direction. The increase in the relative turbulence intensity behind the groyne crest in figures 5.6 and 5.7 indicates that the fluctuations in the velocity signal relative to the mean flow velocities are significantly larger than anywhere else in the measurement area. It is reasonable to assume that this can be explained by the presence of a flow separation layer as a result of divergence of the streamlines behind the groyne crest. A flow separation layer is a region where generally speaking the flow velocities are lower and the turbulent fluctuations are higher compared to regions with developed flow conditions.

There are two distinct differences between figures 5.6 and 5.7. First, the magnitude of the relative turbulence intensity behind the groyne crest is a factor of two larger in figure 5.6. Second, the peak in relative turbulence intensity is located more downstream for the streamlined groynes compared to the reference groynes. This might indicate that the separation point for the streamlined groynes is also located further downstream for the streamlined groynes. This is a logical explanation for the increase in discharge capacity over the groyne in the streamlined situation compared to the reference situation.

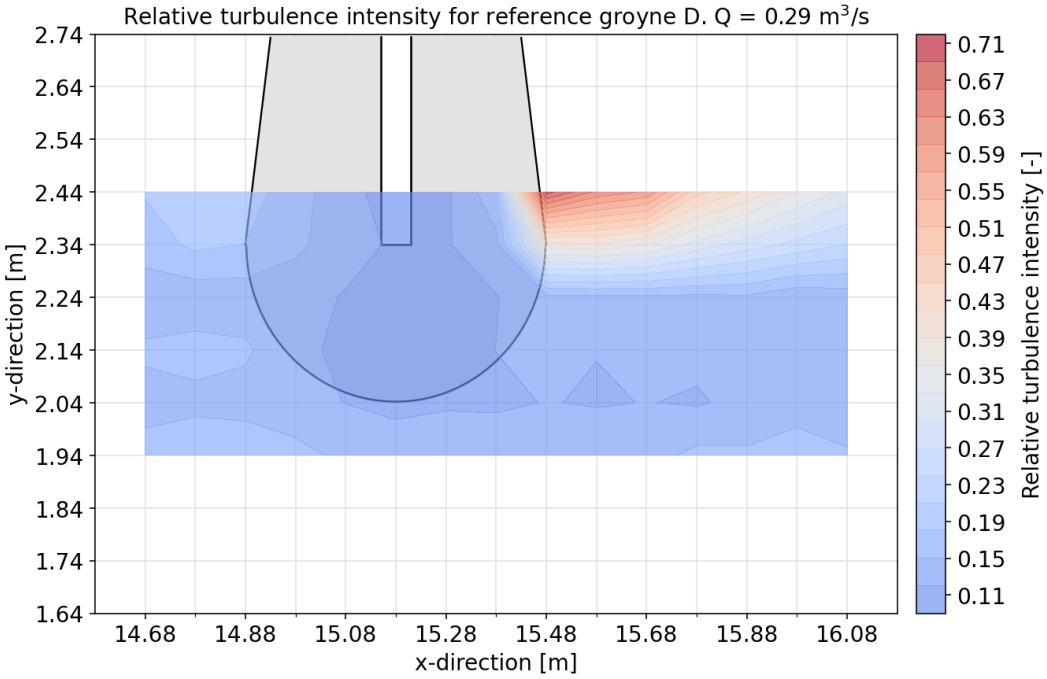

Figure 5.6: Contour plot of the relative turbulence intensity around the groyne tip of reference groyne D. Note that the scale of the color bars for both figures are the same, however, the limits are different. This means these figures can be directly compared. The relative turbulence intensity is calculated at around 40 % of the local water depth of each measurement point.

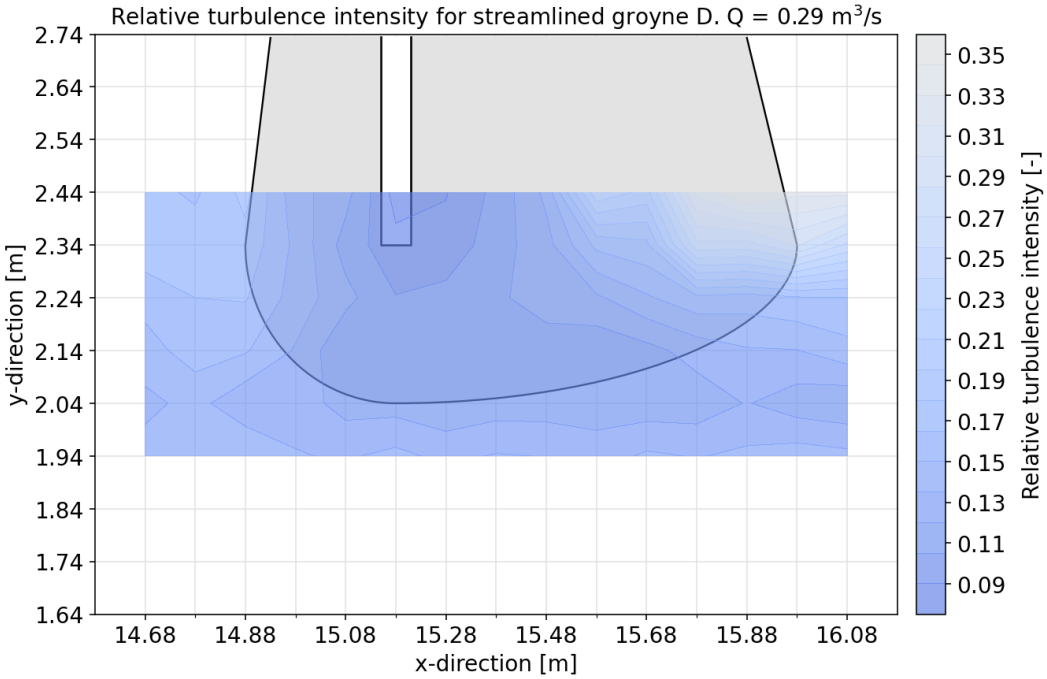

Figure 5.7: Contour plot of the relative turbulence intensity around the groyne tip of streamlined groyne D.

Another possibility to identify reoccurring large-scale turbulent structures, is to use the auto-correlation function ($\mathbf{R}$) and the power spectral density (PSD) function. Large-scale turbulent structures have a great impact on morphological changes near groynes (Yossef, 2004). Streamlining groynes might have an impact on these large-scale turbulent structures. The subject of large-scale turbulent structures is also interesting

based on the fact that Harms (2021) and Yossef (2004) found completely different results in a comparable model set-up using comparable measurement techniques. Harms (2021) found that there were no large-scale turbulent structures present anywhere in the flume. Yossef (2004) found a slow periodic behaviour with a period of around 25 seconds at all measurement locations between two groynes.

Both results are surprising as the expected period of any large-scale turbulence would be in the order of a couple of seconds, given the model set-up and hydraulic conditions.

Figures 3.7 and 3.8 show that enough locations are available to analyse large-scale turbulence. The results from Yossef (2004) can be compared by analysing the cross-section between groynes. The auto-correlation and PSD functions at these locations can clarify the intensity and extent of the mixing layer between main channel and groyne fields and compare the results between a reference and streamlined groyne. Figure 5.8 shows the auto-correlation functions for some locations along transact 35, or at x $= 24\ m$, for both the reference and streamlined groynes.

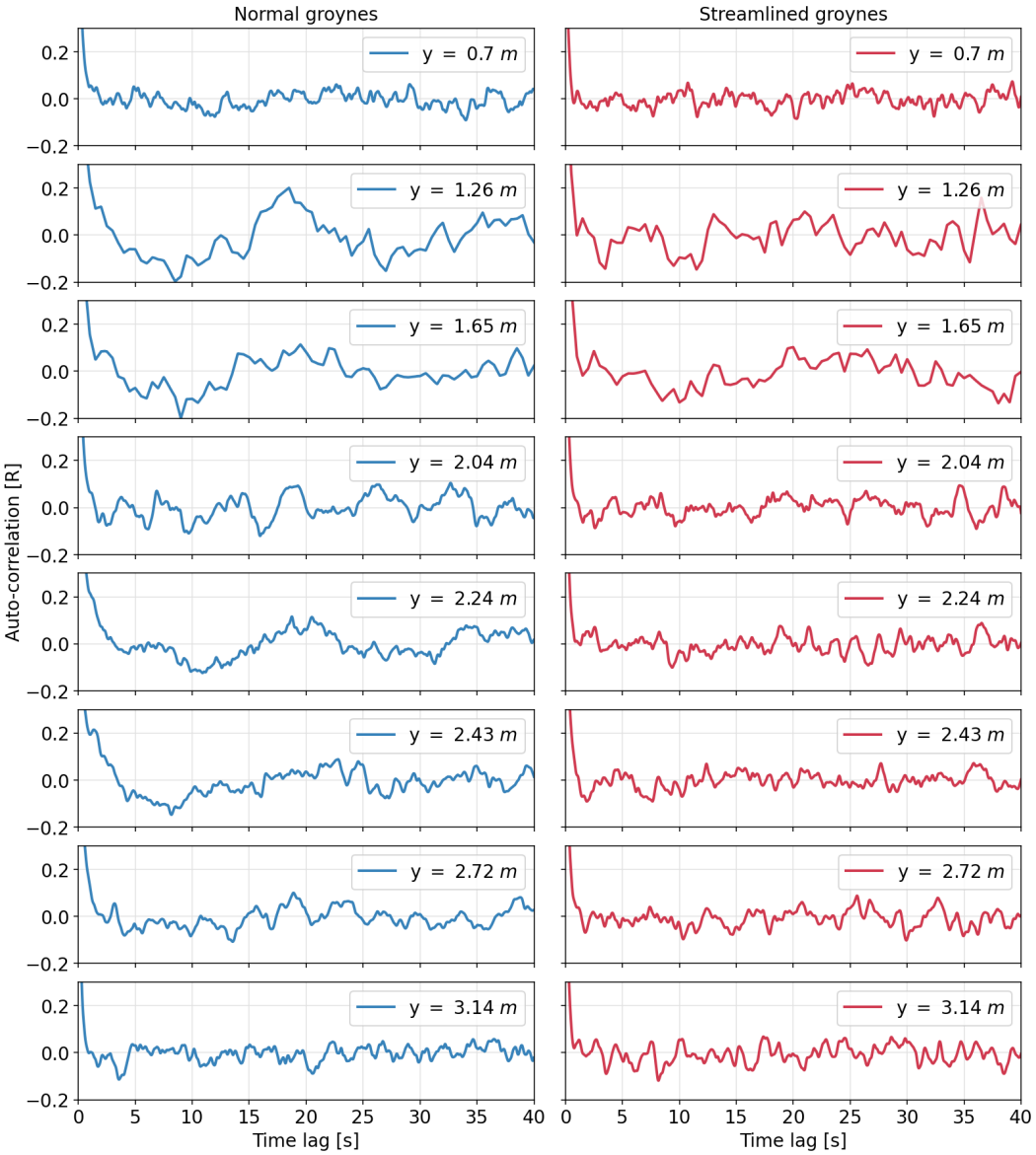

Figure 5.8: Auto-correlation functions along transact 35. The total measurement duration is five minutes. The auto-correlation functions are calculated for the velocity signal in transverse direction minus its mean value.

When analysing figure 5.8, there seems to be a distinction between small oscillatory motions with a period of around two seconds and larger motions with a period between ten and twenty seconds. The transition between the small and the large motions might indicate the effect of the mixing layer between the main channel and the groyne field. Yossef (2004) linked the presence of large turbulent structures to the extent of the mixing layer. Combining this statement with the results from figure 5.8 would suggest that for both the reference and streamlined groynes, the influence of the mixing layer is noticeable at y = 1.26 m but not at y = 0.70 m. So the mixing layer extends to somewhere between these measurement points. In the groyne field, the mixing layer seems to extend till between y = 2.72 m and y = 3.14 m for the reference groynes, and till between y = 2.04 m and y = 2.24 m for the streamlined groynes. Furthermore, the period and the amplitude of the large oscillatory motions seem smaller for the streamlined groynes. In other words, this might indicate that the intensity of the mixing layer is smaller for the streamlined groynes compared to the reference groynes. However, the extent of the mixing layer into the groyne field might also interfere with the effect of the downstream flow separation zone or the vortex shedding from the groyne tip.

Just like downstream flow separation, the presence of a mixing layer (compared to a 1D compound channel model) is associated with energy losses and a subsequent decrease of the total discharge capacity of the river section. Within the boundaries of this experiment, it is expected that the decrease in relative turbulence intensity, as presented in this section, has a greater effect on reducing the groyne-induced resistance. A reason might be that the turbulent structures resulting from the mixing layer do not negatively impact the flow carrying water depth, as is the result from the downstream flow separation. However, it is difficult to substantiate this presumption in a quantitative manner, as these effects can not be isolated using the data at hand.

Unfortunately, the PSD functions do not return a clear dominant frequency to substantiate the claims made in the paragraph above, even with sufficient overlap for the Fast-Fourier-Transform (FFT) method. This is likely because of the many sub-harmonics in the signal. It is not clear whether Yossef (2004) or Harms (2021) did any post-processing on the signal to remove this "noise".

The use of auto-correlation and PSD functions is limited for this research. The auto-correlation functions were useful for the transacts between groynes to examine the intensity and extent of the mixing layer. However, when plotting the auto-correlation function for the measurements around the groyne tip, it is not possible to identify any underlying pattern that could distinguish the flow over and around a reference or streamlined groyne. This does not mean that there are no identifiable oscillatory motions visible in the signal. For the detailed measurements around the groyne, there was a large variation in the periods of the oscillatory motions, ranging from around 1 - 25 seconds.

5.5 Summarising flow velocity data

Streamlining groynes increases the flow velocity and specific discharge over the crest of the groyne. This difference is around 5 % over a large portion of the length of the groyne. Flow separation downstream of the groyne is reduced compared to reference groynes. It is difficult to accurately quantify this reduction, mainly due to the uncertainty in the size of the separation layer for the reference groynes. By using auto-correlation functions the extent of the mixing layer was assessed. In the main channel, the extent of the mixing layer was identical for both situations, but in the groyne field, the turbulent structures resulting from the mixing layer extended further into the groyne field for the reference groynes.

6 | Discussion

Chapters 4 and 5 presented and interpreted the results for the experimental research. This chapter aims to better contextualise the results from the previous chapters by analysing the uncertainties and comparing the results to previous researches.

6.1 Uncertainty analysis

In experimental research, uncertainties in the measurement techniques and in the data processing are inevitable. For the results to be usable, it is important to be aware of these uncertainties and quantify them if possible. This uncertainty analysis focuses mainly on the uncertainties in the various data processing steps, which are especially relevant for the flow velocity measurements. The uncertainties in the measurement equipment and measurement techniques like the EMF meters and the laser altimeters are already discussed in subsections 3.3.1 and 3.3.2.

6.1.1 Flow velocity measurement points

The first uncertainty when processing the flow velocity data is embedded in equation 3.1. However, it is unknown what the accuracy of the transformation formula is, which is the reason this possible uncertainty is not further elaborated on.

The second uncertainty is related to the time induced drift from the zero-offset of the EMF meter signals. As stated in subsection 3.3.2, this time induced progression was measured with a short measurement before and after each measurement run. Theoretically, the progression curve can take any arbitrary combination of shape and magnitude during a measurement run (as this can not be measured when the flow velocity in the flume is not zero). However, it is reasonable to assume that it follows a roughly linear trend and stays within the range of values measured before and after each measurement run for the entire duration. The magnitude of the time induced progression error turned out to be structurally below $10^{-2}\ m/s$, either in the positive or negative direction. The actual error is unique for every (x, y, z) measurement point. However, for the sake of simplicity, the error for every (x, y, z) measurement point is set constant at $\pm\ 10^{-2}\ m/s$. This is on the safe side, and therefore justified.

When obeying the strict mathematical rules, it is unfortunately not possible to quantitatively improve the accuracy of these measurements using the statistical property where the variance of the sum of n measurements is equal to n times the variance of a single measurement. This is prohibited by the fact that not all measurement points are measured by the same EMF meter and also because of variations in local hydraulic conditions between consecutive measurement points. However, at an arbitrary (x, y) coordinate, the measurements are conducted by the same EMF meter. Additionally, the variations in local hydraulic conditions are expected to have a minimal effect on the time induced progression error of the EMF meters as this is not dependent on the flow velocity of the water flowing around the probe of the EMF meter.

Therefore, it is deemed justified to use this statistical property.

To calculate the resulting error, one has to divide the error of a single measurement by the square root of the number of measurements, which, in case of this experiment, is either three or four. This results in an error that is consistently below $5.7 \cdot 10^{-3}\ m/s$ for the (x, y) coordinates with three measurements over the vertical and an error which is consistently below $5.0 \cdot 10^{-3}\ m/s$ for the (x, y) coordinates with four measurements over the vertical. With the uncertainty known, it is possible to calculate an upper and lower bound for the depth-averaged flow velocity.

6.1.2 Vertical flow velocity profile

In section 5.1 is explained how the depth-averaged flow velocities are calculated. The main uncertainty when calculating the depth-averaged flow velocity is related to the curve that is fitted through the measured data. The ability to fit a curve through the data is mainly dependent on two characteristic properties of a curve fit method: the amount of data points available through which a curve can be fitted and the standard mathematical function used to approach the velocity profile.

For subcritical flow in an open channel it is customary to use a logarithmic function to represent the somewhat logarithmic flow velocity profile. Figure 5.1 shows the results of these curve fit methods. To verify the validity of these curve fit methods, a 0^{th} order verification is used. This method uses the trapezoidal integration method with linear extrapolation from the lowest available measurement point to the bed level (where the flow velocity is set at 0 m/s) and an extrapolation with constant flow velocity from the highest available measurement point to the water surface level.

For illustrative purposes, figure 6.1 shows the result of the 0^{th} order verification for the same measurement points as used in figure 5.1. For actual conclusions regarding the applicability of an exponential curve fit, more measurement points were used to substantiate the conclusions.

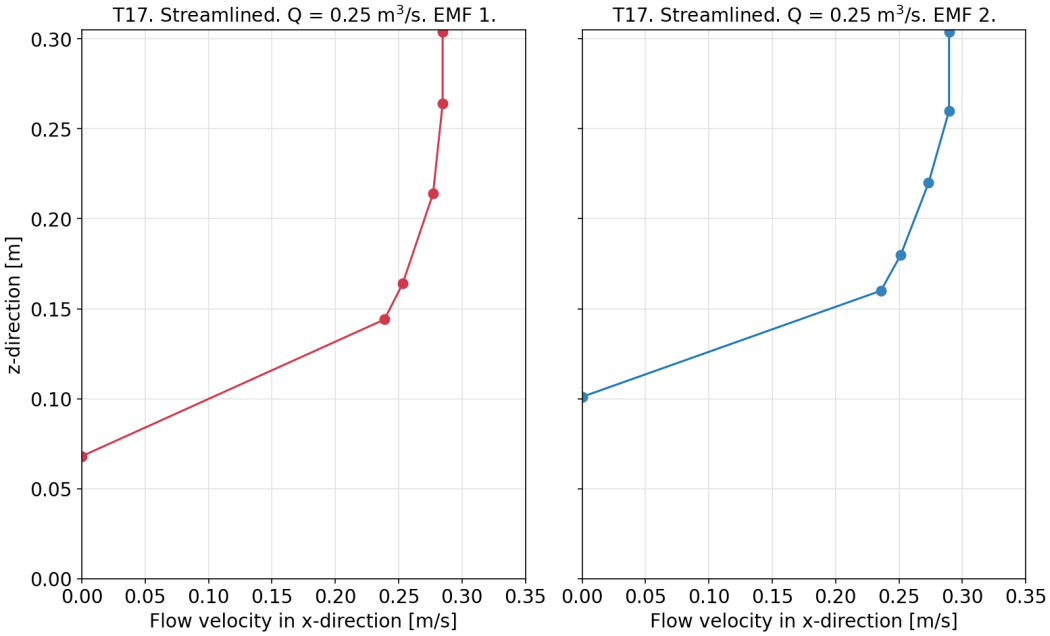

Figure 6.1: Plot of the flow velocity profile in z-direction for two EMF meters spaced 10 cm apart in y-direction under the same hydraulic conditions. In this figure, the curve fit method is replaced by the 0^{th} order verification described above.

Using the 0^{th} order verification method displayed in figure 6.1 results in a decrease of around 15 % to 25 % in the depth-averaged flow velocity in the main channel measurement points compared to the curve fit method. This decrease of 15 % to 25 % is consistent throughout most of the measurements. The substantial magnitude of this difference indicates that the data is sensitive to the depth integration method of choice. Given the context of these measurements, especially considering the low measurement density near the bed level, such a difference is to be expected and can be explained. The linear interpolation from the bed level to the lowest measurement point increases the share of this lower region in the depth-averaged flow velocity calculation compared to an exponential fit. Furthermore, the constant extrapolation from the highest measurement point to the water surface level decreases the share of the last cell in the trapezoidal integration method. Reducing the sensitivity of the data to the choice of depth integration method will be achieved by using more equally spread out measurement points over the water depth and preferably by having a higher concentration of measurement points near the bed level, as this is where the increase in flow velocity is maximum.

This raises the discussion on which of the two depth integration methods is better suited for the data at hand. Below, both methods are compared to each other.

- An advantage of the 0^{th} order method is that it is applicable to any velocity profile, regardless of its shape. This is not the case for the curve fit method, as this method is bound by the limits between which a specified standard function can fit through the measurement points. Figure 6.2 shows an example of this phenomenon. It is clear that using the curve fit method would result in large uncertainties regarding the reliability of the fit. The curve fit method would disregard the fact the the flow velocity does not increase with increasing water depth.

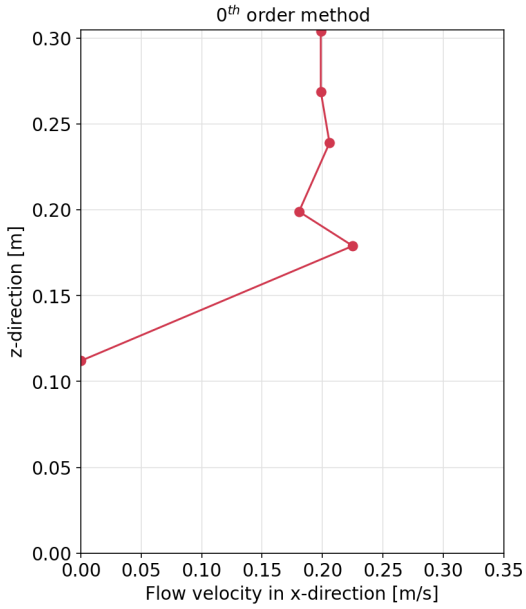

Figure 6.2: Flow velocity profiles showing 0^{th} order method for a velocity profile by the upstream boundary.

This phenomenon is especially present close to the upstream boundary of the flume. The most likely explanation is the fact that the skewed discharge distribution at the upstream boundary results in an excess of discharge at the floodplain side of the flume. This causes flow conditions that are far diverted from an equilibrium flow, resulting in flow velocity profiles like in figure 6.2. When considering all measurement points, around 25 % of all velocity profiles are unable to accept an exponential

curve fit. However, this gives a distorted picture of the entire data set as 90 % of the data points that do not accept an exponential curve fit are located in the first three and last two transacts of the flume, i.e. transacts 31, 38, 32, 43 and 37 from figure 3.8. Therefore, it is advised to only use the area between x = 9 m and x = 30 m for flow analysis when using the curve fit method.

- A disadvantage of both methods is that they can lead to significant errors if the measurement points are not closely spaced. Within the boundaries of this research, this is probably the explanation for the high sensitivity of the data to the chosen depth integration method, as explained below figure 6.1.

- An advantage of the curve fit method is that it takes the shape of the velocity profile into account. However, it is important to have a sufficient understanding of the expected shape of the velocity profile before using the curve fit technique, i.e. this means that the curve fit method is less suited for locations where a non-logarithmic flow velocity profile, e.g. figure 6.2, is present. Of course this also applies to the 0^{th} order method if the measurement points are not closely spaced.

Based on these arguments, it is difficult to state that one of these methods is decisively better suited. For the results analysis in chapters 4 and 5, the curve fit method was used. The reasoning is that the curve fit method gives a better representation of the flow velocities in the lower water column. This is especially true in the main channel. This is despite the low measurement resolution in this part of the water column.

Choosing a depth integration method is especially difficult at the crest of the groyne. The water level at the groyne crest is only 10 cm. As stated in subsection 3.5.1, the EMF meters have to be spaced 3 cm above the bed level and 3 cm below the water surface. This leaves a space of only 4 cm between which is measured. For consistency reasons, the curve fit method was also used for these points. Figure 6.3 shows the flow velocity profile for the same measurement point in y-direction for four consecutive groynes.

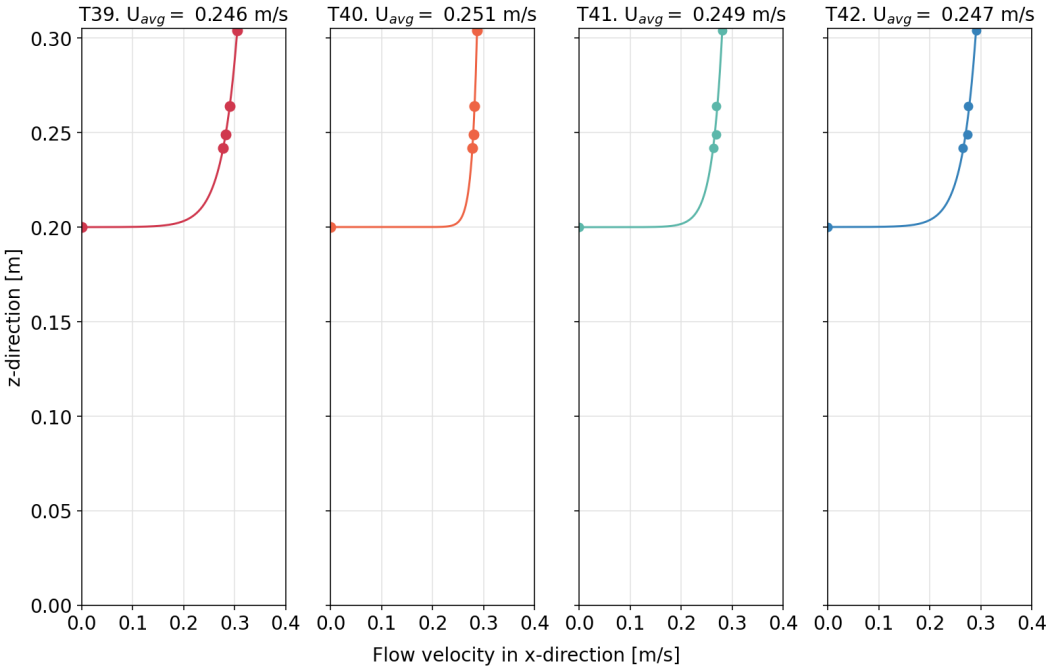

Figure 6.3: Flow velocity profiles for the same measurement point at y = 3.37 m for groynes B, C, D and E.

Figure 6.3 shows that applying the curve fit method for the calculation of the depth-averaged flow velocity leads to comparable results between consecutive groynes. Furthermore, due to the large gradient in the velocity profiles in figure 6.3, it follows that the difference between the curve fit method and the 0^{th} order

method is even larger. When considering the results from figure 6.3, a modified version of the 0^{th} order method, where the linear interpolation between the lowest available measurement point and the bed level is replaced by an extrapolation with constant flow velocity from the lowest measurement point to the bed level. The problem is that this method leads to worse results in the main channel. Therefore, this method is not further investigated.

Getting a consistent results makes this method applicable when looking for embedded patterns within the data set. This is, of course, only true when aware of this error. Furthermore, the flow field over the groyne crest has to show similar characteristics over each consecutive groyne.

Being unable to select a superior method for the calculation of the depth-averaged flow velocity will have a negative impact on the usability of the data for numerical modelling, as a consistent error of unknown magnitude is present. This might incline the numerical modeller to unjustifiably adjust certain model parameters like the bed roughness to get a better resemblance between the experimental data and the numerical model.

6.2 Discharge verification

Considering the results from chapter 4 and 5 and the uncertainties described in section 6.1, it is possible to plot the development of the total discharge over the length of the flume (conform figure 2.9) as a verification of the consistency of the data (note: not the accuracy). As stated in subsection 6.1.2, it is only possible to calculate the discharge between transacts 39 and 36 from figure 3.8, i.e. between x = 9 m and x = 30 m. Moreover, due to the lack of measurement points in the floodplain and part of the main channel, the total discharge is calculated between y = 0.30 m and y = 3.85 m. This causes the calculated discharges to be smaller than the total discharge in the flume. Figure 6.4 shows the results.

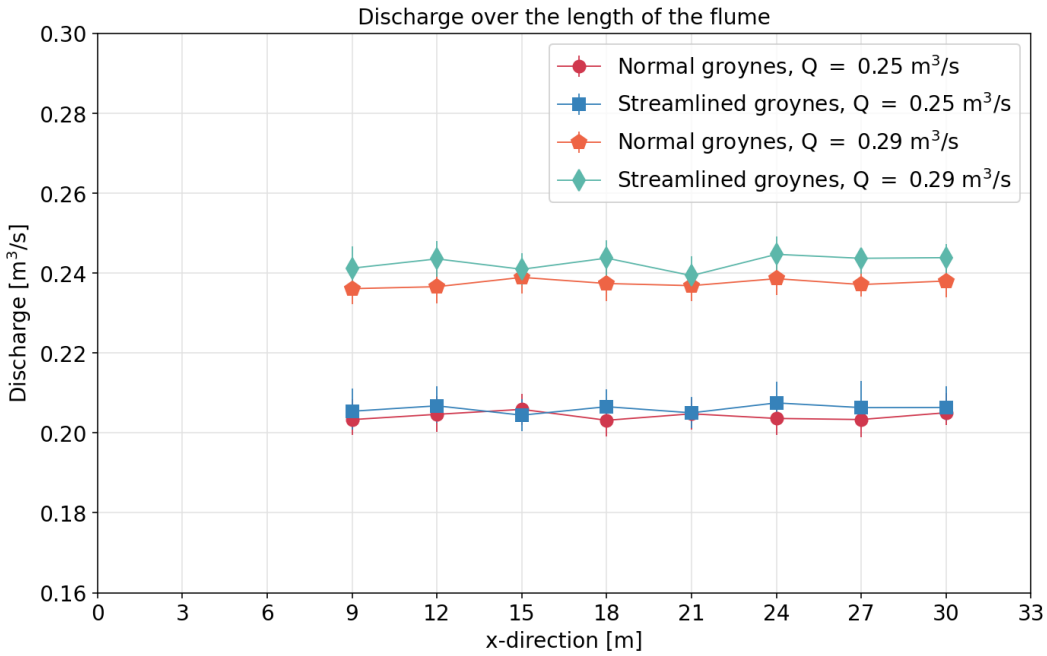

Figure 6.4: Graph of the discharge over the length of the flume for discharges of 0.25 m^3/s and 0.29 m^3/s. Note that the first nine meters and the last four meters are not included. The reason is also explained in subsection 6.1.2.

The maximum deviation of the discharge in figure 6.4 is less than 2 %. This is an extra conformation of the consistency of the data set. This figure is directly comparable to figure 2.9 made by Chavarrías (2022), based on the data set from Harms (2021). Note that figure 2.9 is the result of numerical simulations from Chavarrías (2022) which were based on the data from Harms (2021). This is also explained in subsection 2.5.1.

Given the knowledge obtained during this experimental research, more can be said about the resulting inaccuracies found by Chavarrías (2022). His numerical model started at x = 0 m in the flume. As explained in subsection 6.1.2, this can lead to an inaccurate estimation of the measured upstream discharge, especially when using the curve fit method for the calculation of the depth-averaged flow velocity. However, this can also be the case with the 0^{th} order method. Figure 6.2 shows that in some cases, the flow velocity is higher at lower points in the water column. When the amount of measurements over the vertical is insufficient, such a phenomenon might go unnoticed. This leads to inaccurate estimations of the depth-averaged flow velocity. However, this phenomenon is barely present between x = 9 m and x = 30 m, as stated in subsection 6.1.2 (this is of course only true when assuming that the measurement density over the vertical is sufficient for this experiment). So two options that might improve the modelling results are to only model between x = 9 m and x = 30 m or to get an even larger data set from which it can be confidently concluded that all flow processes and anomalies are captured within the data.

6.3 Bed roughness estimation

As described in subsection 2.5.2, accurate measurements of the bed roughness are difficult to obtain. This section aims to elaborate on various methods available for the calculation or validation of the bed roughness using the obtained flow velocity and water level data from this research. For simplification, it is desirable to approximate the river section (in the case of this research, the flume) as a 1D compound channel. This method is also used by Harms (2021). This section initially focuses only on the main channel, as this is where the flow is best represented by a logarithmic velocity profile corresponding to fully developed flow conditions. Figure 6.5 shows the cross-section of the main channel in the flume.

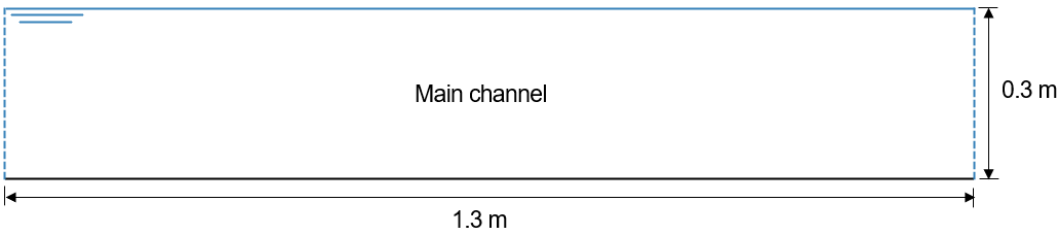

Figure 6.5: Cross-section of the main channel of the flume.

The definition of the cross-section for which the bed roughness is calculated can have a major impact on the result. It is important that the hydraulic conditions are constant over the area of the cross-section, as well as having as few unknown parameters as possible. The width of the cross-section is defined from y = 0.3 m to y = 1.6 m. This is to exclude the effect of the wall (which would unnecessarily complicate the calculation of the bed roughness) and the mixing layer between the main channel and the groyne field.

Two methods are used to calculate or verify the bed roughness in the main channel. Later in this section, the limitations and boundaries of these formulas are explained. The first method is proposed by Harms (2021), which is a balance between the water level slope, the bed shear stress and the advection. It solves equation 6.1 to obtain the unknown parameter.

$$-\frac{\partial h}{\partial x} = \frac{g \cdot Fr_{mc}^2}{C_{mc}^2} \cdot \frac{1}{1 - Fr_{mc}^2} \quad with \quad Fr = \frac{U}{\sqrt{g \cdot h_{mc}}} \quad and \quad C = 18 \log\left(\frac{12 \cdot R}{k_s}\right) \tag{6.1}$$

The second method is proposed by Rijkswaterstaat. The goal of this formula is not to get the definitive value of the bed roughness, but more to connect the shape of the vertical flow velocity profile to the bed roughness and to identify the presence of boundary layer flow. Formula 6.2 is used for this calculation.

$$C_{log-fit} = \frac{\sqrt{9.81}}{0.41} \frac{\sum\left(\ln\left(\frac{z_i}{h_{mc}}\right) + 1\right)^2}{\sum\left(\ln\left(\frac{z_i}{h_{mc}}\right) + 1\right)\left(\frac{u_i}{U} - 1\right)} \tag{6.2}$$

In equation 6.1 and 6.2:

- Fr_{mc} $[-]$ Froude number in the main channel.
- C_{mc} $[m^{1/2}/s]$ Chézy roughness value in the main channel.
- U $[m/s]$ depth-averaged flow velocity.
- h_{mc} $[m]$ Main channel water depth.
- R $[m]$ Hydraulic radius.
- k_s $[m]$ Bed roughness height.
- u_i $[m/s]$ The measured flow velocity value in cell with index *i*.
- z_i $[m]$ Height above the bed of cell with index *i* (with measured flow velocity u_i).

First, equation 6.1 is considered to get an estimate for the bed roughness in the main channel. The bed roughness is calculated at transact 35 at x = 24 m (figure 3.8) for both the reference and streamlined groynes with a discharge of 0.25 and 0.29 m^3/s. This location is used for three reasons. First, the water level measurement density is highest around this region, this is desirable for the calculation of the local water level slope. Second, the effect of the boundary conditions is as small as possible and the last reason is that the flow at a transact between two groynes experiences minimal acceleration and deceleration in streamwise direction, which results in a constant local water level slope (figure 4.1). The unknown parameter in equation 6.1 is the bed roughness height k_s.

Table 6.1 shows the results of calculating the roughness height using equation 6.1 for both depth integration methods.

Table 6.1: Resulting roughness parameters using equation 6.1. In the index column, 0.XX is the discharge in m^s/s, N = normal / S = streamlined is the groyne type and CF = curve fit / 0^{th} is the depth integration method. The colors are indicators for figure 6.7.

	Roughness height (m)	**Chézy** $(m^{1/2}/s)$	**Manning** $(s/m^{1/3})$
0.25, N, CF	0.0132	42.2699	0.0194
0.25, N, 0^{th}	0.0358	34.5111	0.0237
0.25, S, CF	0.0127	42.5712	0.0192
0.25, S, 0^{th}	0.0358	34.5229	0.0237

0.29, N, CF	0.0204	38.8595	0.0210
0.29, N, 0^{th}	0.0469	32.3976	0.0253
0.29, S, CF	0.0214	38.4941	0.0213
0.29, S, 0^{th}	0.0483	32.1087	0.0255

The values in table 6.1 are the average values over the four measurement points in the main channel. It is remarkable that the Chézy coefficients for the high discharge are lower than for the lower discharge. This is caused by the presence of additional flow processes in the flume. To prove this, consider a hypothetical case where the influence of these additional flow processes are negligible and take into account the fact that the water level at this specific streamwise coordinate does not vary enough to cause significant differences. In this case, the change in local water level slope should in theory compensate the higher flow velocities belonging to the higher discharge, resulting in constant roughness parameters for both discharges.

There is also a clear difference between both depth integration methods. The Chézy coefficients for the 0^{th} order method are around 15 to 20 % smaller compared to the curve fit method. This difference is likely caused by the limited number of measurement points lower in the water column. Due to the nature of the 0^{th} order method, as explained in subsection 6.1.2, this causes an underestimation of the depth-averaged flow velocity compared to the curve fit method. Keeping all parameters constant, a lower depth-averaged flow velocity results in a lower Chézy coefficient, i.e. a rougher bed profile.

The bed level in the flume consists of gravel with a D_{n50} of 8 mm. The last part of equation 6.1 shows how Colebrook & White (1937) derived the Chézy roughness C from the roughness height k_s and the hydraulic radius R. In this relation, a rule of thumb is to choose the roughness height to be between two and three times the D_{n50} of the bed. Based on this rule of thumb, it is reasonable to assume that the calculated values, at least in the main channel, are realistic.

Surprising is the large deviation with the results from Harms (2021). He calculated the roughness height in the main channel to be 0.042 ± 0.002 m and in the groyne field to be 0.012 ± 0.002 m. One would expect the roughness height in the groyne field to be larger than in the main channel due to the presence of the groynes. Two differences between the results from Harms (2021) and this research are the effect of the wall and the usage of the hydraulic radius instead of the water depth. However, these differences do not explain the large difference in results between both researches.

What can be an explanation for the large difference in results between both researches is the chosen water level slope. For this research, the local water level slope was used corresponding to the transact around which the roughness height was calculated. Harms (2021) used the average water level slope over the entire length of the flume. As stated in section 4.2, the flow in the flume has to adjust to equilibrium conditions. Therefore, it is difficult to determine a single value for the water level slope that corresponds to the entire flume. The water level measurements in this research show that the water level slope at the beginning of the flume is somewhat steeper than at the end of the flume (see table 4.1). This leads to an overestimation of the water level slope when using a single value for the entire flume, which in turn results in an overestimation of the roughness height when using equation 6.1.

As stated above, equation 6.2 uses the shape of the vertical velocity profile to identify boundary layer flow. In this formula, it is possible to use both the 0^{th} order method and the curve fit method.

For the 0^{th} order method to be used in equation 6.2, the velocity profile between two measurement points is approximated by a straight line. Therefore, the index i is equal to the number of measurement

points in the vertical plus two $(n + 2)$, accounting for the points at the bed level and water surface.

To account for the curved shape of the velocity profile from the curve fit method, the velocity profile is divided into much smaller sections by making use of the predetermined parameters of the curve fit.

Figure 6.6 compares the results for both depth integration methods in equation 6.2. For the reasons explained above, the only points at which the roughness was determined for both methods are located in the main channel at transact 35 (x $= 24\ m$). Determining the roughness at other locations results in deviations that can not solely be assigned to the differences between the two methods.

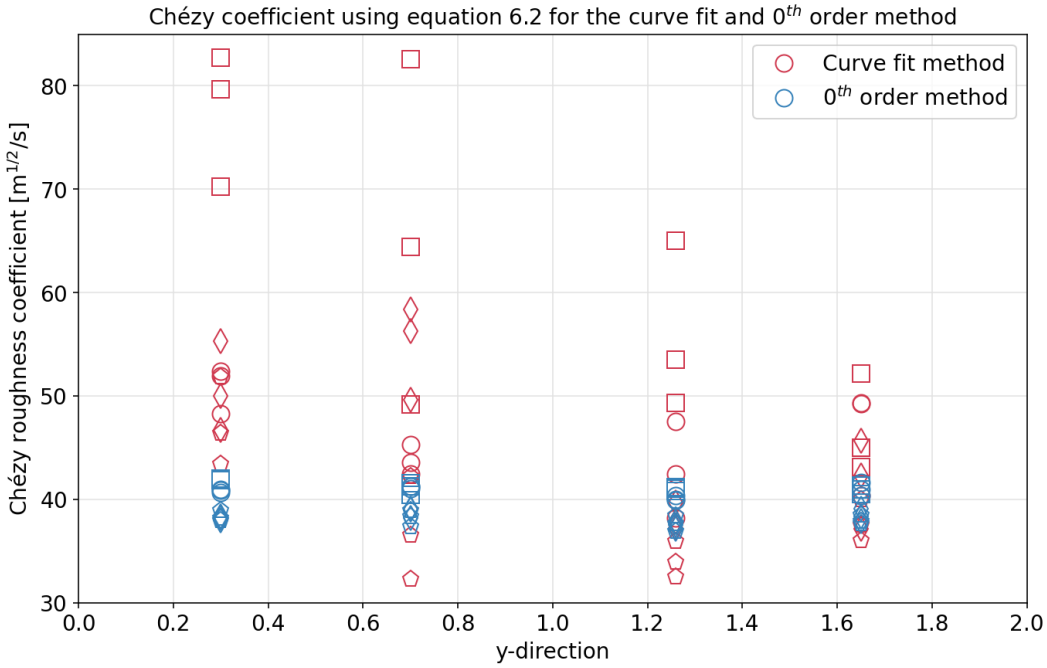

Figure 6.6: Comparison of equation 6.2 for both depth integration methods. The different marker styles each represent a different hydraulic condition. All measurement points for this graph are located in the main channel part of the flume. This means that the water level for each of these points is the same.

Figure 6.6 shows a clear difference between both depth integration methods in equation 6.2. The 0^{th} order method is much more consistent than the curve fit method. This means that even though the curve fit method is consistent for the calculation of the depth-averaged flow velocity, as explained in subsection 6.1.2, the inconsistency regarding the shape of the velocity profile makes it unsuited to be applied to equation 6.2. Therefore, the 0^{th} order method is preferred to investigate the presence of boundary layer flow in the flume.

Figure 6.7 shows the same data as figure 6.6, but is adjusted to display the results from the 0^{th} order method in a more detailed manner. Figure 6.7 also adds the results from equation 6.1.

The blue markers in figure 6.7 show that, just like equation 6.1 in table 6.1, there is a clear difference between the low and high discharge. This difference is in the same order of magnitude for both equations and depth integration methods. The blue markers corresponding to equation 6.2 fit better to equation 6.1 in combination with the curve fit method. This is surprising considering that both use a different flow velocity profile.

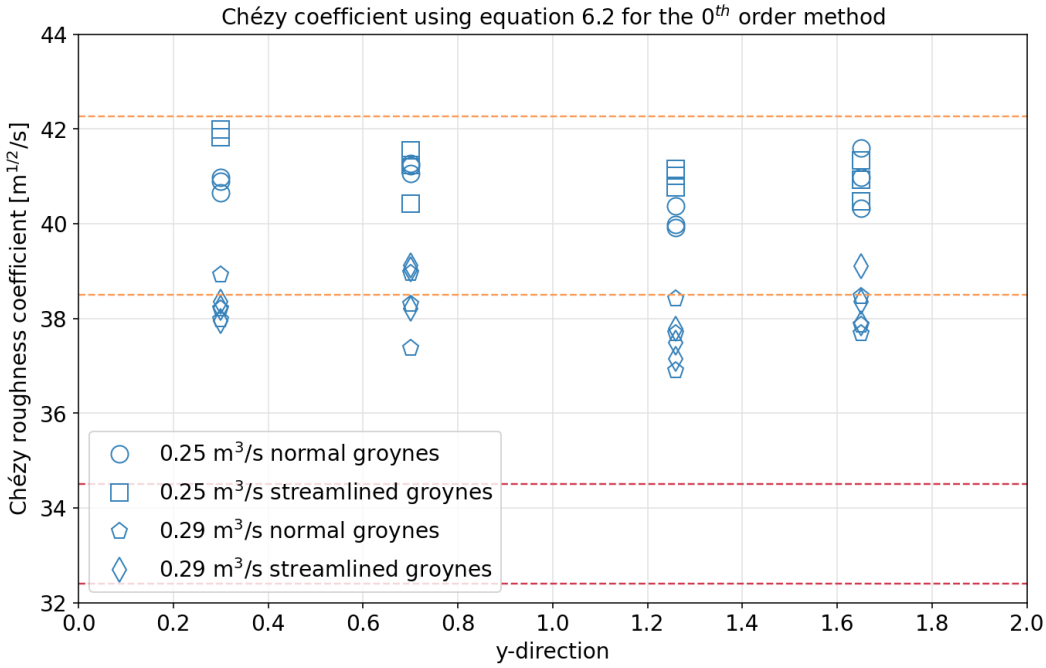

Figure 6.7: Chézy roughness coefficients calculated using equation 6.2 for the 0^{th} order method. The orange lines correspond to the values in table 6.1 for the curve fit method (orange columns) and the red lines correspond to the values for the 0^{th} order method (red columns). The upper line of each color is for the low discharge and the lower line is for the high discharge.

Figure 5.2 shows that for y $= 0.3\ m$ till y $= 1.26\ m$ the flow velocity increases for an increasing transverse coordinate and than decreases again at y $= 1.65\ m$. This is completely the opposite of the blue markers in figure 6.7. This is surprising, as one would expect that an increase in flow velocity would result in a higher C, given all other parameters remain constant.

Now that the behaviour of equation 6.2 is analysed, it is possible to identify the presence of boundary layer flow in the flume. Boundary layer flow is interrupted when the resulting Chézy coefficient shows a significant deviation from the values in figure 6.7. It is important to note that equation 6.1 is unsuited for the calculation of roughness parameters at locations where no boundary layer flow is present, as this equation is based on developed flow conditions. The agreement between equations 6.1 and 6.2 proves the presence of boundary layer flow in the main channel.

As stated by Rijkswaterstaat, equation 6.2 is useful to qualitatively describe the presence of boundary layer flow in an open channel. In other words, the relevant information that can be extracted from equation 6.2 is related to the rate of change of C, not the absolute values.

The combination of equation 6.2 with the linear approximation between vertical velocity points and the limited number of measurement points low in the water column makes this method unsuited to be used in areas with flow separation (e.g. downstream of the groyne). However, this is not a problem as the presence of flow separation automatically indicates the absence of boundary layer flow.

The presence of boundary layer flow in the main channel was already established. The groyne tip measurements (subsection 3.5.1) show that boundary layer flow is still present at y $= 1.94\ m$ throughout the whole width of the groynes. The measurements also show that boundary layer flow was already reestablished at the transacts in the middle of the groyne fields (figure 3.8). The results around the groynes show significant variations between consecutive measurement points, indicating to the absence of boundary layer flow.

6.4 Limitations of the model set-up

It is important to be aware of the effects that the physical boundaries and limitations of the flume have on the interpretation of the results of the physical model experiment and how these boundaries affect the extrapolation of these results to real-world scenarios. Some of these limitations have already been addressed in previous chapters. This section gives a complete overview of the limitations of the model set-up.

- The limited length of the flume of 40 m and the influence of the boundary conditions prevent the development of equilibrium flow conditions. In this sense, the flow is said to be in equilibrium when the flow pattern is completely repetitive for each consecutive groyne. The absence of equilibrium flow conditions complicates a consistent estimation of the water level slope for the entire flume. This problem is also addressed in chapter 4.

- The walls of the flume exert a friction force on the flow. This reduces the flow velocity near the walls which is unrealistic for flow in a main channel or a floodplain in a river. The walls can also compromise the resulting horizontal mixing layers between the main channel and the groyne field and between the groyne field and the floodplain. This is of course only relevant if the mixing layer would extend beyond the physical boundaries of the flume. Section 5.4 concluded that half way through a groyne field, this is not the case for the main channel - groyne field mixing layer. However, it is unknown whether this is also true for the groyne field - floodplain boundary.

- The main channel : groyne field : floodplain ratio in the flume is equal to 2 : 2 : 1, with a total width of 5 m. This does not represent cross-sections in a Dutch river. Conventional cross-sections in the river Waal, which formed the basis for this experiment, have a typical main channel : groyne field : floodplain ratio of 2 : 1 : 10 with a total width of around 1.3 km (the total width of an actual cross-section can vary greatly depending on the width of the floodplain. For the Pannerdensch canal this ratio is different with a much smaller floodplain). This results in an overestimation of the share of the groyne field in the flume compared to an actual river cross-section. In other words, in an actual river cross-section, the influence of streamlining groynes is smaller than measured and observed in the flume.

6.5 Comparison to literature

Now that the results and the boundaries between which the results can be interpreted are known, it is possible to compare the results to other literature. The main focus of this section is to compare the results from this research to the research of Harms (2021) as the model set-up and measurement techniques are nearly identical.

In his thesis, Harms (2021) compared the behaviour of the flume without groynes to a situation with reference groynes, with a downstream slope of 1:3. He set the downstream water level to 0.38 m and varied the upstream discharge from 0.174 to 0.255 to 0.284 m^3/s. This research uses a downstream water level of 0.30 m and upstream discharges of 0.230, 0.250, 0.270 and 0.290 m^3/s (section 3.2. The situations with reference groynes and discharges of 0.250 and 0.290 m^3/s can be directly compared to the results from Harms (2021), with the only significant difference being the water level.

When comparing the water level slopes over the whole length of the flume, decreasing the downstream water level from 0.38 to 0.30 m results in a three times higher water level slope for both discharges (comparing table 4.1 with figure 3.3). Even though these results are consistent, more comparable data needs to be acquired to find an actual relation between the water level and the water level slope in the flume.

Figure 6.8 shows how Mosselman & Struiksma (1992) approximated the shape of the water level slope over groynes and in the main channel. They stated that the average water level slope in the groyne field should match that of the main channel and that the water level drop over a groyne is compensated by a milder water slope between consecutive groynes to obey this statement.

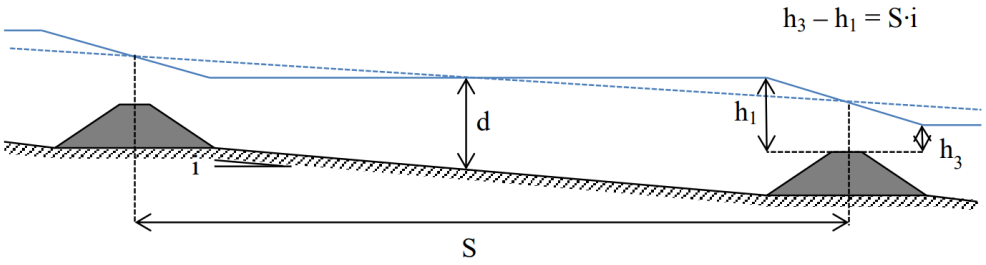

Figure 6.8: Development of the water level slope in the main channel and the groyne fields. Source: Mosselman & Struiksma (1992).

Figure 6.8 shows clear differences with figure 4.1. The main difference is the absence of the large water level drop over the crest of the groyne. This was an essential approximation for the schematisation in a 1D model without lateral mass and momentum exchange with a spatial grid coarser than the distance between groynes, Mosselman & Struiksma (1992). For the measurements, the resulting water level drop over a groyne is in line with the water level slope in the main channel. The result is that the water level slope in the main channel is equal to the water level slope between two groynes.

While the measured water level slopes are in line with realistic conditions found in rivers, the size of the model set-up is a lot smaller. This might explain why Mosselman & Struiksma (1992) stated there to be a clear difference between the water level slope in the main channel and the groyne fields, which was not found in the measurements.

One of Harms' (2021) main findings was the presence of a region with lower surface velocities between y $= 2$ m and y $= 3$ m over the whole length of the PTV measurement area (between x $= 12$ m and x $= 25$ m. He also observed these lower flow velocities at x $= 25$ m using EMF meters. It is unclear whether the results from the EMF meters showed this phenomenon at other locations in the flume.

The measurements from this research showed that a region with lower flow velocities was observed around the groyne tip (figure 5.2). In the groyne fields, this local decrease in flow velocity was not present. Moreover, the region with lower flow velocities seems to be more present for the streamlined groynes. Harms (2021) stated that the origin of this phenomenon is difficult to uncover using the available data. This is also true for this research and Harms' (2021) explanation that this is probably caused by secondary circulations is still the most likely.

As discussed before, Chavarrías (2022) used the experimental data from Harms (2021) in a numerical model. Figure 6.9 shows a plot of the specific discharge over the width of the flume for the experimental results from Harms (2021) and the numerical results from Chavarrías (2022).

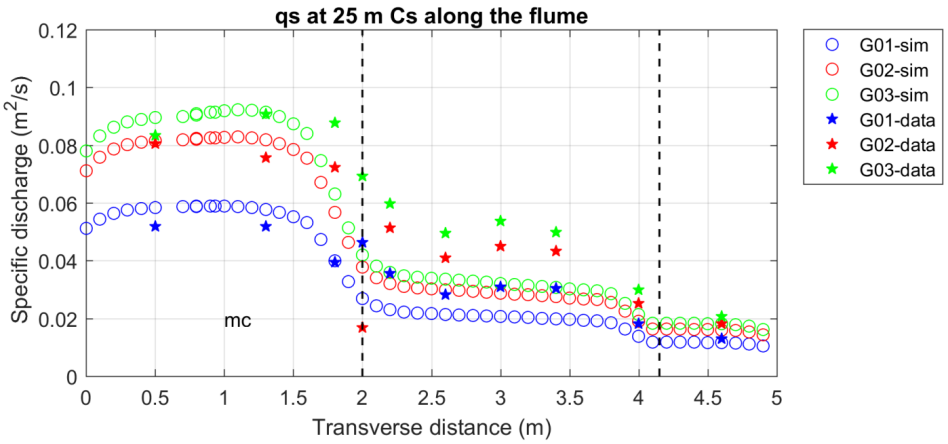

Figure 6.9: Specific discharge over the width of the flume comparing experimental and numerical results. Source: Chavarrías (2022).

It seems like the experimental data from this research (figure 5.3) better agrees with the numerical data by Chavarrías (2022) than with the experimental data by Harms (2021). However, be aware that the water level during Harms' (2021) experiments was higher than for this research. An increased water level given a constant discharge results in lower flow velocities over the whole cross-section and a different discharge distribution between the main channel and the groyne field. This is because the ratio of the water depth in the groyne field over the main channel increases for a higher downstream water level. In other words, the fact that the results from this research agree better with the numerical models from Chavarrías (2022) might be due to the difference in hydraulic conditions.

Ambagts (2019) did a numerical investigation on lowering and streamlining groynes based on data from a physical model experiment from BAW. Be aware that the geometry of this experiment was different compared to the geometry in this research. Ambagts (2019) was able to model the various flow processes that characterise the flow over and around a groyne. These flow processes were also measured and observed in this research. An interesting agreement between this research and the results from Ambagts (2019) is the fact that he found the height of the flow separation zone to exceed the height of the groyne.

Ambagts (2019) investigated the effect of streamlining the groyne by decreasing its downstream slope. Regarding the flow separation zone, he concluded that a downstream slope of 1:5 still resulted in flow separation, but a downstream slope of 1:10 did not show any flow separation. The streamlined groynes in this research used a downstream slope of 1:8, where, conform figure 5.7, flow separation was still present, albeit less extreme than for a reference groyne with a downstream slope of 1:3. Ambagts (2019) also concluded that streamlining the downstream slope of a groyne results in a marginal reduction of the groyne-induced resistance, especially when compared to lowering the crest height of a groyne. In this research, the streamlining groynes results in a 5 % increase of the discharge capacity over the crest.

7 | Conclusions and recommendations

7.1 Conclusions

The objective of this research was to gather experimental data on the effect that streamlining the groyne by decreasing its downstream slope has on the reduction of the overall resistance of a straight river section and how the general flow characteristics differ from a situation with reference groynes.

The first research goal was to **quantify the change in overall water level slope in the river section and display the results in such a way that it is possible to draw clear and objective conclusions regarding the effectiveness of streamlining groynes in rivers.**

It was hypothesised that based on the change in water level slope, it would be possible to get an accurate quantification of the effect of streamlining groynes. It turned out that due to the 3D characteristics of the flow and the possibility for water to flow around the groyne, the effect of streamlining did not manifest itself by means of a change in water level slope that was to be solely assigned to the effect of streamlining.

The effect of streamlining was notable when analysing the flow velocity data. Within the boundaries of this experiment, the effect of streamlining was expressed by a redistribution of the discharge over the width of the flume. The increase of the flow velocity and the discharge capacity over the crest of the groyne was around 5 %, although this difference was not spaced equally over the groyne crest, i.e. at the groyne field - floodplain boundary the specific discharge even showed a slight decrease for the streamlined groynes. These results were consistent for all measurement conditions, with the exception of the transacts near the upstream and downstream boundary.

The water level data showed that the water level drop over, and the local water level slope near the groyne crest were larger for streamlined groynes. This indicates a larger absolute flow velocity over, and more acceleration near the crest of the groyne. This increase in flow velocity over the crest of the groyne was also measured by the EMF meters. The total increase in flow velocity was around 5 %, with the exception at the groyne-floodplain boundary.

The second research goal was to **use the gathered flow velocity data from the scaled river section, and more specifically from around the groyne tip, to get better insight in, and to analyse the flow over and around groynes and to draw conclusions on how this flow differs for streamlined groynes compared to reference groynes.**

The flow field around the groyne tip shows a consistent increase of the depth-averaged flow velocity throughout the measurement area. The highest flow velocities were observed at the transverse coordinate were the groyne transitions into the normal bed level. Furthermore, the flow direction at the upstream slope of the groyne was more extreme for the streamlined groynes. Downstream, the reference groynes show a rapid change in flow direction changing from aimed towards the main channel to aimed to the groyne field.

The relative turbulence intensity was used to analyse the effect of streamlining groynes on the intensity of the turbulence around the groyne tip. Contour plots from around the groyne tip showed that the relative turbulence intensity showed a significant increase behind the groyne crest. This increase likely indicates the presence of downstream flow separation behind the groyne. Two differences were observed between the reference groyne and the streamlined groyne. First, the magnitude of the relative turbulence intensity was a factor of two larger for the reference groyne compared to the streamlined groyne. Second, the peak of the relative turbulence intensity was located more downstream for the streamlined groyne. This might indicate that the separation point for the streamlined groyne is located more downstream compared to the reference groyne.

The auto-correlation functions were used to identify the region of influence of the horizontal mixing layer between the main channel and the groyne field. It was found that three meters downstream of the groyne, the extent of the mixing layer in the main channel was the same for both the reference and streamlined groynes. In the groyne field, it was found that the mixing layer extended less far into the groyne field for the streamlined groynes. The difference was around 0.5 m in transverse direction.

Summarising, the main effect of streamlining the downstream slope of a groyne is an increase of its discharge capacity of around 5 %.

7.2 Recommendations

The bullet list below is a list of recommendations that could improve the measurement efficiency and accuracy, given the experience gained during this experiment regarding physical model research.

- For future research under comparable circumstances it is recommended to measure the flow velocities closer to the bed level. Consider the situation at the groyne crest, where the local water level was 10 cm (for reasons explained in subsection 3.3.2). The water level of 10 cm in combination with the physical limitations of the EMF meters, caused that the 3 cm above the bed level and the 3 cm below the water surface could not be measured, leaving only 4 cm in which the measurements were conducted. The problem is that in the 3 cm above the bed level, the largest flow velocity gradient is expected. To better capture the large velocity gradients, two options are available. If the water depth is left at 10 cm at the groyne crest, different measurement equipment has to be used to measure the flow velocity. However, this is expensive and not preferable. Another option is to increase the water level and the discharge in the flume. The higher discharge compensates the higher water level which would otherwise decrease the Froude number at the groyne crest. The advantage of the higher water level (lets say 20 to cm at the groyne crest) is that the measurable water depth increases (the 3 cm above the bed level and the 3 cm below the water surface remain immeasurable, resulting in 14 cm of measurable water depth instead of 4 cm). This gives a better understanding about the shape of the flow velocity profile.

- Regarding detailed measurements, like the groyne tip measurements (subsection 3.5.1), it is recommended to space the EMF meters a few cm further apart. This has two reasons. First, a larger spacing between EMF meters (lets say 15 cm apart instead of 10 cm) enables the researcher to cover a larger area with the detailed measurements without losing much detail. The second reason is that with a 10 cm spacing, the calibration of the EMF meters is a very sensitive and time consuming process. This phenomenon is less present when EMF meters are spaced further apart. This can result in significant time savings, especially considering the fact the EMF meters were re-calibrated every time the rela-

tive position of the probes changed with respect to the bed level. It was found that re-calibrating the EMF meters was less necessary when the EMF meters were spaced far apart, i.e. during the flume measurements (subsection 3.5.2).

- This point is closely related to the first two points. During this research it was found that the 0^{th} order depth integration method was more stable and reliable that the curve fit method. However, the 0^{th} order method resulted in a consistent underestimation of the depth-averaged flow velocity due to the limited number of measurements in the vertical. By increasing the number of measurements in the vertical (say from 4 to 8), the significant underestimation of the 0^{th} order method will decrease, as the flow velocity profile will more closely match that of the actual flow velocity profile. This way, the 0^{th} order method can be used throughout the whole research, resulting in more consistency which improves the quality of the conclusions. The extra measurements in the vertical can be compensated by eliminating the first three and the last two transacts.

References

Alavian, V. & Chu, V.H. (1985). *Turbulent exchange flow in shallow compound channel.* Proc., 21st IAHR Congress, Melbourne, Austra-lia, 446–451.

Ambagts, L.R. (2019). *Flow over and around submerged groynes: Numerical modelling and analysis of a groyne flume experiment.* [MSc. Thesis] Delft University of Technology.

Anzifar, H. (2010). *Flow resistance and associated backwater effect due to spur dikes in open channels.* University of Saskatchewan, Saskatoon.

Barishnikov, N.B. & Ivanov, G.V. (1971). *Role of flood plain in flood discharge of a river channel.* Proc. 14th IAHR Congress, Paris, France, 141-144.

Bazin, H. (1888). *Expériences Nouvelles sur l'Ecoulement par Déversoir.* Mémoires et Documents, Annales des Ponts et Chaussées 6, pp 393-448.

Bloemberg, G. (2001). *Stroomlijnen van zomerkaden.* [MSc. Thesis] Delft University of Technology.

Bos, M.G. (1989). *Discharge measurement structures.* 3rd Ed., ILRI Publication 20.

Brater, E.F. & King, H.W. (1976). *Handbook of hydraulics, for the solution of hydraulic engineering problems.* 6th edition, McGraw-Hill, Inc.

Chavarrías, V. (2022). *Improving the modelling of flow over groynes: Modelling of laboratory cases.* Deltares, Delft.

Colebrook, C.F. & White, C.M. (1937). *Experiments with Fluid Friction in Roughened Pipes.* Proceedings of The Royal Society A: Mathematical, Physical and Engineering Sciences, 161, 367-381.

Deltares. (2020). *Instrument, Programmable electromagnetic liquid velocity meter.* [Manual]. Deltares, Delft.

Fritz, H.M. & Hager, W.H. (1998). *Hydraulics of embankment weirs.* Journal of Hydraulic Engineering, Vol.124, No.9.

Harms, J.M. (2021). *Physical modelling of submerged groynes.* [MSc. Thesis] Delft University of Technology.

Hoffmans, G.J.C.M. (1992). *Two-dimensional mathematical modelling of local-scour holes.* [PhD. thesis] Delft University of Technology.

Knight, D.W. & Shiono, K. (1990). *Turbulence measurements in a shear layer region of a compound channel.* Journal of Hydraulic Research, Vol.28, No.2.

Kruijt, M. (2013). *Resistance of submerged groynes.* [MSc. Thesis] Delft University of Technology.

Limerinos, J.T. (1970). *Determination of the Manning Coefficient From Measured Bed roughness in Natural Channels.* GEOLOGICAL SURVEY WATER-SUPPLY PAPER 1898-B.

Malekzadeh, F., Salmasi, F., Abraham, J. & Arvanaghi, H. (2022). *Numerical investigation of the effect of geometric parameters on discharge coefficients for broad-crested weirs with sloped upstream and downstream faces.* (Appl Water Sci 12, 110). *https://doi.org/10.1007/s13201-022-01631-5.*

Mosselman, E. & Struiksma, N. (1992). *Effecten van kribverlaging.* WL | Delft Hydraulics, Delft.

Sieben, J. (1999). *Energieverliezen bij zomerkaden - theoretische verkenning.* (99.151.x). RIZA.

Sieben, J. (2003). *Gestroomlijnde zomerkaden, de invloed van het dwarsprofiel op energieverliezen bij overlaten.* (2001.113x). Ministerie van Verkeer en Waterstaat, Rijkswaterstaat, Directie Oost-Nederland.

Sofialidis, D. & Prinos, P. (1999). *Numerical study of momentum exchange in compound open channel flow.* Journal of Hydraulic Engineering, Vol.125, No.2.

Uijttewaal, W.S.J. (2003). *Turbulence in hydraulics.* [lecture notes] Delft University of Technology.

Uijttewaal, W.S.J. (2005). *Effects of Groyne Layout on the Flow in Groyne Fields: Laboratory Experiments.* Journal of Hydraulic Engineering, Vol.131, No.9.

Van Broekhoven, R.W.A. (2007). *Het effect van kribverlaging op de afvoercapaciteit van de Waal ten tijde van hoogwater.* [MSc. Thesis] Delft University of Technology, Koninklijke Boskalis Westminster nv, Hydronamic.

Van Prooijen, B.C. (2004). *Shallow mixing layers.* [PhD. thesis] Delft University of Technology.

Van Prooijen, B.C., Battjes, J.A. & Uijttewaal, W.S.J. (2005). *Momentum Exchange in Straight Uniform Compound Channel Flow.* Journal of Hydraulic Engineering, Vol.131, No.3.

Van Schijndel, S. & Jagers, B. (2001). *Anticiperend onderzoek kribben: rekenen rondom kribben met HLES.* WL | Delft Hydraulics, Delft.

Villemonte, J. R. (1947). *Submerged weir discharge studies.* Engineering news record, 139(26), 54-56.

Yossef, M.F.M. (2004). *The effect of the submergence level on the resistance of groynes, an experimental investigation.* Advances in Hydro science and-Engineering, Proc. of the 6^{th} Int. Conf. on Hydro science and Engineering CD-ROM, Brisbane, Australia.

Yossef, M.F.M. (2005). *Morphodynamics of rivers with groynes.* Delft University Press, Delft.

Appendix: water level measurements

This appendix provides all the extra information and data from the water level measurements. Figure A.1 shows the same data as figure 4.1, but without the inclusion of the rail deflection. Figure A.1 shows the water level measurements for two additional transverse locations.

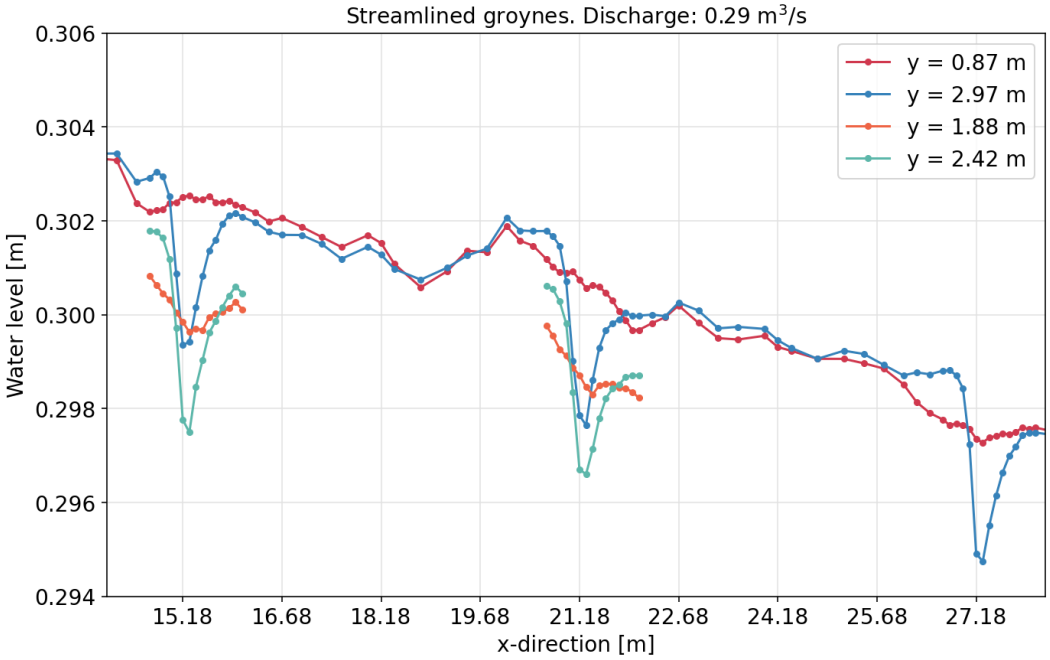

Figure A.1: Water level measurements for the streamlined groynes with a discharge of Q $= 0.29\ m^3/s$.

For this research, only two laser altimeters were available. Figure A.1 shows the problem when trying to measure the water level at more than two locations in the transverse direction and the importance of conducting all water level measurements in the same run. There are two problems that make the measurement data from y $= 1.88\ m$ and y $= 2.42\ m$ incomparable to the other water level measurements.

The first problem is related to the downstream water level. The downstream water level varies slightly every time the flume is turned on. This is due to the qualitative set-up method for the downstream water level. This is an insignificant problem if the water level data is only used to calculate the specific discharge for example. However, if the goal of the water level measurements is to make a plot like in figure A.1, a variation of the downstream water level in the order of $10^{-4}\ m$ can negatively affect the usability of figures like figure A.1.

The second problem is related to the relative position in z-direction of the laser altimeters. Given the inaccuracies of the hardware mounting systems, moving the laser altimeters to a different transverse coordinate makes it impossible for the data to be linked to the data for the other transverse coordinates.

The overall shape of the water level profile at y $= 1.88\ m$ and y $= 2.42\ m$ is accurate, as these measurements were conducted using exactly the same measurement method. However, because of the two problems described above, the relative position in z-direction is unknown. There are two options on how this problem can be resolved. The first option is to simply use more laser altimeters. Unfortunately, this was not possible for this research. The second solution is to only move one laser altimeter to a different transverse coordinate without shutting down the flume. This way, when the measurements are done, a zero-measurement with no flow can be conducted. This makes it possible to get the relative position in z-direction of the new measurement point. However, this would only yield one extra measurement point in transverse direction. Moreover, this would double the total measurement duration. This makes it hard to be carried out by a single person, as the current water level data took an entire day to acquire.

Figure A.2 below shows the measured deflection of the rails on which the platform was positioned. This deflection was subtracted from the water level profiles like figure A.1.

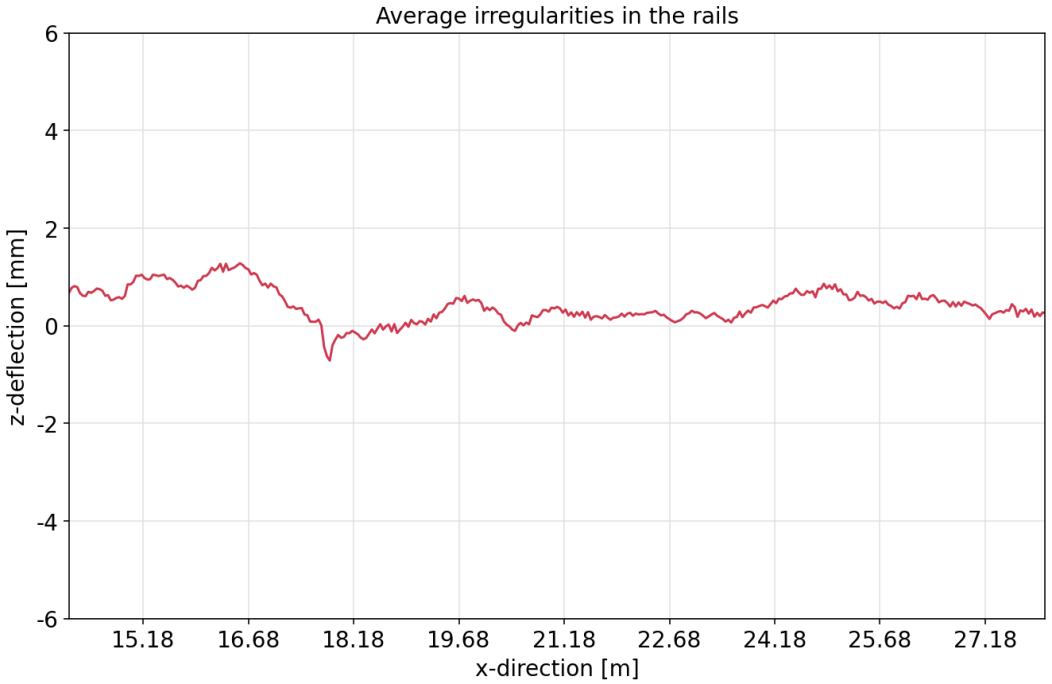

Figure A.2: Deflection in z-direction of the rails on which the platform was positioned.

The measurements were conducted using the water table in the flume as a level. The laser altimeters were connected to a distance wheel. This distance wheel made it possible for the laser altimeters to measure at given intervals in space, instead of time, which is the default setting and also used for the normal water level measurements. The graph in figure A.2 shows the average of multiple passes along the length of the flume.

Figure A.3 on the next page shows the water level profiles for each hydraulic condition and groyne type.

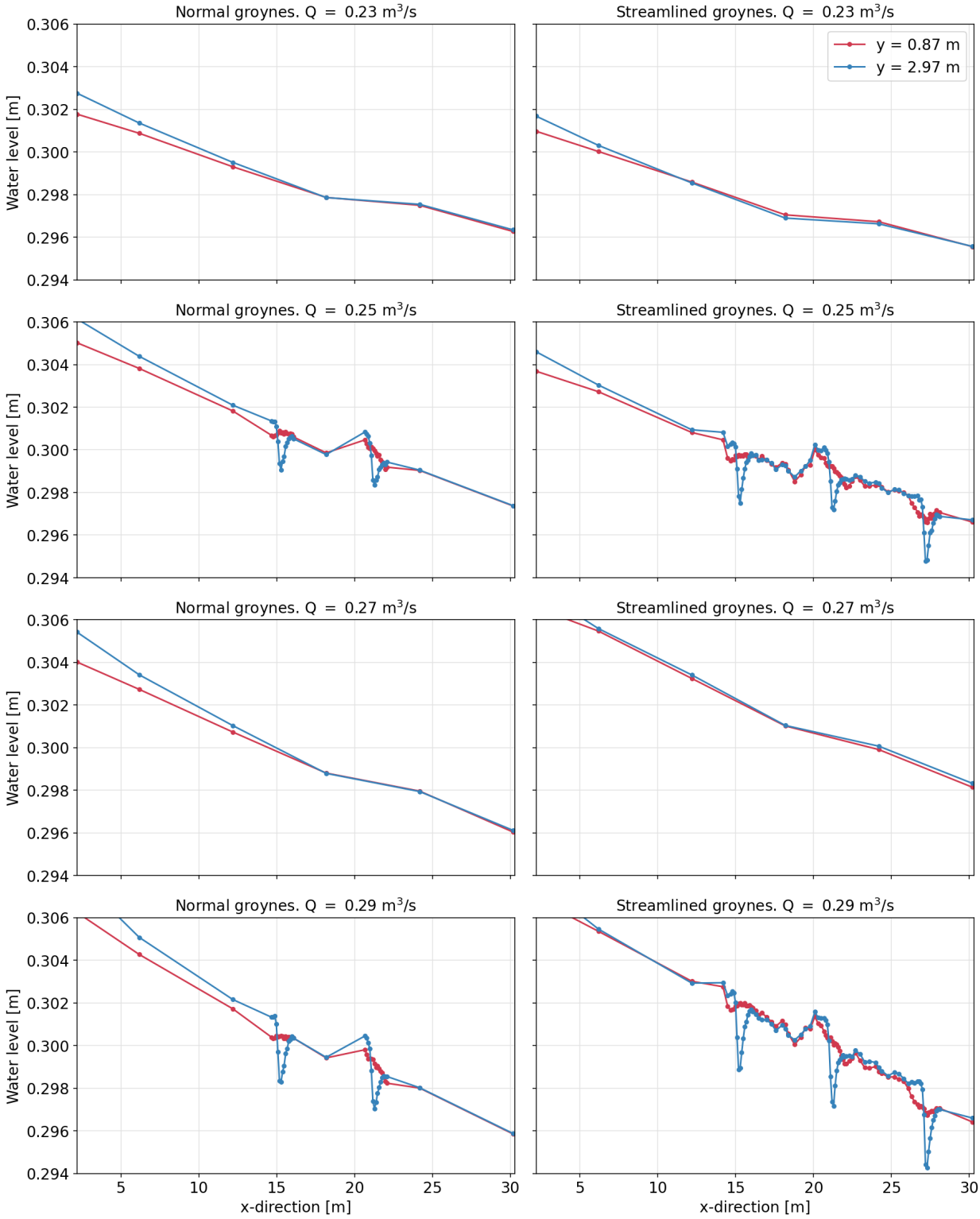

Figure A.3: Water level profiles for all measurement conditions